Energy Conversion and Management: X 29 (2026) 101417

Contents lists available at ScienceDirect

Energy Conversion and Management: X

journal homepage: www.sciencedirect.com/journal/energy-conversion-and-management-x

Combustion mode analysis of a large-bore methanol premixed dual-fuel engine with high methanol energy fractions

Konstantinos I. Kiouranakis [a,*], Robbert Willems [b], Peter de Vos [a], Rinze Geertsma [a,c]

[a] Faculty of Mechanical Engineering, Delft University of Technology, Mekelweg 2, Delft, 2628 CD, The Netherlands
[b] Powertrains Department, Netherlands Organisation for Applied Scientific Research (TNO), Helmond, The Netherlands
[c] Faculty of Military Sciences, Netherlands Defence Academy, Den Helder, The Netherlands

ARTICLE INFO

Keywords:
Diesel engine
Dual-fuel engine
Heavy-duty
Methanol
Combustion mode

ABSTRACT

Methanol has emerged as a promising sustainable fuel for shipping, with the premixed dual-fuel (PRDF) strategy holding strong potential for deploying it in marine internal combustion engines. However, achieving high methanol energy fractions (MEFs) remains challenging due to combustion stability issues, which limit efficiency and operating robustness. Experimental insights into high-MEF operation are scarce, particularly for large-bore engines, leaving critical knowledge gaps in understanding combustion and performance characteristics of methanol PRDF engines. This study addresses these gaps through an experimental investigation on a marine-scale single-cylinder engine, operating with up to 93% MEF and high-load conditions. Two distinct MEF operational ranges were identified, with different mechanisms limiting each boundary. Poor combustion performance and elevated unburned hydrocarbon emissions emerged as the primary factors limiting high MEFs and were more sensitive to pilot ignition timing than to ignition energy. Although energy from premixed combustion Phase I decreased from 25% at 79% MEF to 6.2% at 93% MEF at maximum load, advancing ignition by a shortened ignition delay (from 9.2 °CA to 4.4 °CA) improved combustion efficiency (from 87.9% to 92.7%) and gross indicated thermal efficiency (from 43.4% to 45.3%). A novel framework was applied to analyze heat release profiles, combining qualitative assessment with a quantitative methodology based on two morphology metrics. This approach revealed three distinct combustion modes—characterized by m-, h-, and n-shaped profiles—unique to methanol PRDF operation, each linked to specific underlying mechanisms, and provides a systematic tool for combustion mode classification.

1. Introduction

Long-haul transportation has traditionally depended on reciprocating internal combustion engine (ICE) technology, a reliance that is unlikely to change significantly in the coming years due to the unmatched robustness, high power, and energy density, and efficiency these engines offer compared to alternative power solutions such as fuel cells and batteries [1,2]. To sustain these advantages while addressing environmental concerns, current research is increasingly focused on ICE technology that can employ alternative fuels to power future heavy-duty (HD) powertrains [3,4]. Among the array of alternative fuel options, methanol has emerged as a particularly promising candidate [5,6]. Its scalability, favorable combustion properties, and liquid state at atmospheric conditions make it well-suited for transportation applications [7,8]. Methanol's simple chemical structure and low carbon density further enhance its versatility as it can be produced through various pathways, including renewable methods such as biomass conversion or synthesis using renewable electricity [9].

Methanol-fueled engines further provide environmental benefits by significantly reducing emissions of harmful pollutants like nitrogen oxide (NO_x) and particulate matter (PM) [10]. When renewably produced, methanol offers substantial decarbonization potential for hard-to-electrify sectors such as long-range transportation [11]. In HD engine applications, mixing-controlled compression ignition (CI), i.e., the Diesel engine principle, remains the dominant technology due to its superior efficiency and power density [12]. While methanol can be utilized in numerous alternative combustion strategies as a single fuel in CI engines—such as spark-assisted compression ignition (SACI) [13] and partially premixed combustion (PPC) [14]—dual-fuel (DF) technologies have gained the most attention from industry due to their

* Corresponding author.
E-mail address: K.I.Kiouranakis@tudelft.nl (K.I. Kiouranakis).

https://doi.org/10.1016/j.ecmx.2025.101417
Received 14 October 2025; Received in revised form 10 November 2025; Accepted 20 November 2025
Available online 21 November 2025

Abbreviations

aHRR	apparent Heat Release Rate	HRR_{max}	Maximum Heat Release Rate
aTDC	after Top Dead Center	ICE	Internal Combustion Engine
bTDC	before Top Dead Center	ID	Ignition Delay
BTE	Brake Thermal Efficiency	IMO	International Maritime Organization
CA	Crank Angle	IVC	Inlet Valve Closing
CD	Combustion Duration	IVO	Inlet Valve Opening
CDC	Conventional Diesel Combustion	LB	Lean-burn
CI	Compression Ignition	LD	Light-duty
CL	Combustion Losses	LRF	Low Reactivity Fuel
CMI	Combustion Mode Index	MAPO	Maximum Amplitude of Pressure Oscillations
CO	Carbon Monoxide	MEF	Methanol Energy Fraction
CO_2	Carbon Dioxide	MEP	Mean Effective Pressure
COV	Coefficient of Variance	MPDF	Micro Pilot Dual Fuel
CR	Compression Ratio	NO_x	Nitrogen Oxide
DAS	Data Acquisition System	ON	Octane Number
DF	Dual-fuel	P_{max}	Peak Pressure
DFDC	Dual Fuel Diffusion Combustion	PMR	Phase Magnitude Ratio
DO	Diesel-only	PRDF	Premixed Dual Fuel
EL	Exhaust Losses	PRR	Pressure Rise Rate
EOC	End of Combustion	SACI	Spark Assisted Compression Ignition
EVO	Exhaust Valve Open	SI	Spark Ignition
gIMEP	Gross Indicated Mean Effective Pressure	SOC	Start of Combustion
HD	Heavy-duty	SOI	Start of Injection
HL	Heat Losses	TDC	Top Dead Center
HRF	High Reactivity Fuel	UHC	Unburned Hydrocarbon
HRR	Heat Release Rate		

operational flexibility [15]. These systems can retain the capability to operate solely on diesel fuel when methanol availability is limited, a critical feature for industries like maritime transport [16].

In the DF engine concept, combustion of the low-reactivity fuel (LRF), such as methanol, is enabled by reactivity and ignition control provided by the high-reactivity fuel (HRF), typically diesel [17]. This synergy between fuels enables ignition and combustion control, making DF strategies suitable for HD applications. While alternative DF concepts, such as reactivity-controlled compression ignition (RCCI) and direct dual-fuel stratification (DDFS) [18], have demonstrated great potential in achieving high efficiency levels and significantly lower NOx emissions, their challenges in combustion controllability have limited their commercial adoption. Two primary DF combustion strategies have demonstrated the ability to effectively utilize the reactivity synergy between LRFs and HRFs while maintaining controllability, and have dominated engine research and development:

1. **Dual-fuel Diffusion Combustion (DFDC):** Both fuels are injected at high pressure near top dead center (TDC), resulting in a diffusion-driven combustion mechanism similar to conventional diesel combustion (CDC).
2. **Premixed Dual-fuel (PRDF):** Methanol is introduced into the cylinder via air path injection (API), forming a premixed air-fuel mixture that is ignited by a HRF, such as diesel. This ignition process mimics the role of a spark plug in spark-ignition (SI) engines and aims to lead to flame propagation akin to Otto-cycle combustion.

Because achieving the highest possible methanol utilization is a key objective in DF engine development, most practical applications—particularly in large marine engines—have prioritized the DFDC concept [19,20]. For these large-bore engines, for which space and design constraints are less restrictive for the selected injection strategy, DFDC provides a viable pathway for methanol utilization, leveraging its robust diffusion-driven combustion mechanism. However, for a wide range of engine sizes, such as high-speed four-stroke marine and locomotive engines, DFDC presents significant challenges. These engines often face spatial constraints in the cylinder head that complicate the integration of additional injection systems necessary for DFDC operation. The high-pressure fuel system required for injecting methanol further limits its applicability as a diesel engine retrofitting option. This limitation underscores the importance of PRDF strategies as a more practical and flexible solution for methanol utilization across an extended spectrum of engine sizes. As such, PRDF represents a critical area of research for expanding methanol's role as a sustainable fuel in HD powertrains.

However, the PRDF combustion strategy faces challenges stemming from the complex interplay of multiple combustion mechanisms inherent to this concept [21]. The combustion process in PRDF engines involves an initial phase of premixed diesel combustion, followed by the autoignition of methanol that becomes entrained within the diesel flame or is in the flame's immediate vicinity. Subsequently, multiple turbulent flame fronts propagate throughout the remaining methanol–air mixture. The relative contributions and interactions of these mechanisms are highly sensitive to the ratio of LRF to HRF, a parameter that fundamentally shapes the resulting combustion regime and is expected to exhibit different sensitivities across varying engine loads [15]. The intricate interplay of these combustion mechanisms in PRDF engines has a substantial impact on the occurrence of abnormal combustion events, with direct consequences for efficiency and emissions performance. The use of methanol as the LRF introduces further complexity due to its pronounced cooling effect, which alters ignition and flame propagation dynamics in ways that differ from other gaseous LRFs like methane. These additional sensitivities underscore the need for a deeper understanding of methanol-specific PRDF combustion phenomena. This could further support ongoing research efforts to address unregulated pollutants associated with methanol operation, such as unburned methanol and formaldehyde, which are primarily linked to incomplete oxidation and wall-wetting phenomena [15]. Although these species were not measured in the present work, this study discusses the underlying combustion inefficiencies that contribute to their formation.

Experimental studies on methanol PRDF engines, particularly at higher MEFs, remain limited, with most research constrained to moderate MEFs due to combustion challenges. This scarcity is especially pronounced for large-bore HD engines. Cung et al. [22] investigated the methanol PRDF strategy in a HD single-cylinder engine with a bore size of 131 mm. This study revealed that knock challenges limit MEF to 49.4% under high-load operation of 23.5 gIMEP and 1200 rpm. Dierickx et al. [23] demonstrated stable operation at the highest MEF of 84% in a six-cylinder high-speed marine engine with a bore size of 108 mm using single-point injection strategy. Zhao et al. [24] retrofitted a single-cylinder diesel engine setup with a bore size of 100 mm to explore the effect of the injection timing of both high-pressure directly injected methanol and diesel fuel on the combustion mode. When the combustion mode shifted to premixed with early methanol injection configurations, MEF was limited to 50%. Overall, to the best of the authors' knowledge, methanol PRDF applications barely achieve MEF greater than 80% [15,19]. However, recent experiments have demonstrated the feasibility of attaining these higher MEFs, even in large-bore engines (bore > 130 mm). For example, Splitter et al. [25] reported feasible maximum MEFs greater than 75% across the full operating load range at 1800 rpm in a 145 mm bore single-cylinder engine using the methanol PRDF concept. Similarly, Stenzel et al. [26] conducted single-cylinder experiments with an even larger bore (175 mm), while both studies demonstrated the challenges associated with combustion stability during the transition from diesel-only (DO) to methanol PRDF operation and the associated MEF limitations. Both research efforts reported successful optimization strategies to overcome the MEF constraints, demonstrating how altering boundary conditions, such as charge pressure, temperature, and injection timing, can improve combustion performance and extend the attainable MEFs in large-bore engines. Among various optimization variables, pilot injection timing consistently emerges as a critical parameter for ensuring stable operation and increasing MEF limits.

Despite these recent advances, this study has identified three remaining key research gaps in this field. First, there is a lack of detailed investigation into the transition from DO to methanol PRDF operation at high MEFs. Second, systematic analyses of heat release behavior and conceptual mode classification remain scarce for large-bore PRDF engines, hindering comprehensive understanding of the underlying combustion mechanisms, their interactions, and their implications for engine performance. This gap is especially critical for methanol-fueled engines, as methanol's unique thermophysical properties greatly influence combustion dynamics. Third, an analytical methodology that can assess and quantify combustion characteristics specific to the distinct behavior in methanol PRDF concepts is lacking. Consequently, the operational behavior of large-bore methanol PRDF engines remains poorly understood, a shortcoming that significantly impedes efforts to achieve high MEFs while maintaining diesel-like performance.

This study addresses these research gaps through an experimental investigation on a marine-scale single-cylinder engine featuring a 170 mm bore and a high-pressure methanol port fuel injection system. The elevated injection pressure is designed to enhance methanol evaporation, thereby mitigating combustion challenges typically associated with poor evaporation and mixing, and ultimately expanding the feasible MEF range in PRDF engines. This experimental research demonstrates two MEF operating regimes that appear when transitioning from diesel to methanol operation, and provides results in the high-MEF region constrained by poor combustion performance. Beyond the novelty of the experimental setup and campaign, this work delivers a systematic and in-depth analysis of combustion characteristics and engine performance in methanol-fueled PRDF operation.

The remainder of this paper is structured to directly target the three distinct knowledge gaps, which collectively constrain current understanding of methanol-fueled PRDF engines. Section 2 establishes the necessary conceptual framework for PRDF combustion, providing foundational background for the analysis of the methanol experiments to follow. Section 3 details the experimental setup and test conditions, with Section 4 outlining the data analysis strategy, placing special emphasis on the combustion staging methodology developed to address the unique combustion characteristics and knocking phenomena encountered in PRDF operation. Building upon these foundations and employing the developed methodologies, Section 5 presents and discusses the results from the experimental study on the methanol PRDF single-cylinder engine. In Section 5.1, this research conducts a preliminary comparative assessment of DO versus methanol dual-fuel operation, highlighting fundamental changes in combustion and engine behavior upon transitioning to methanol. This study places particular emphasis on the value of qualitative assessment and systematic characterization of HRR profile morphologies in PRDF engines. Accordingly, Section 5.2 performs an in-depth exploration by examining HRR profile shapes, their underlying mechanisms, and establishing quantitative metrics to classify combustion modes under methanol operation. Section 5.3 then explores the effects of varying MEFs at two high-load points, to better understand the trends in combustion stability and phasing, and their impact on efficiency and emissions across a range of high MEFs. Finally, Section 6 synthesizes the primary findings and offers key recommendations for future research and practical applications. This comprehensive approach aims to generate new insights into the combustion dynamics of methanol-fueled PRDF engines and inform optimization strategies for HD engine applications.

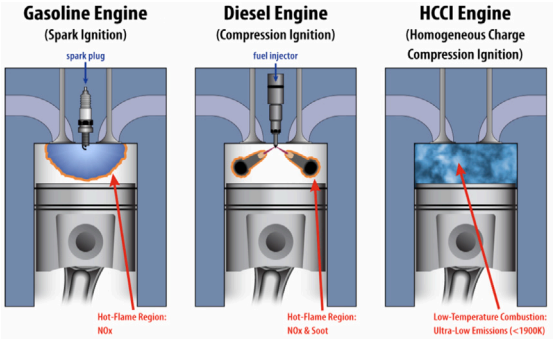

Fig. 1. Combustion modes in three main engine technologies [29].

2. Background on combustion modes

The PRDF concept has become a key strategy for improving emissions performance in ICEs, largely due to its suitability for retrofitting existing engines to run on gaseous alternative fuels and its compatibility with smaller HD engines in which advanced injection concepts like DFDC encounter limitations [4]. The increased adoption of natural gas to reduce NO_x and PM emissions [27], particularly in transport sectors like shipping, led to extensive research in this engine concept. Since most emerging fuels like methanol share combustion characteristics with natural gas, the PRDF strategy, utilizing alternative fuels, remains at the core of engine research [28]. This experience with methane-fueled PRDF engines can provide a valuable foundation for understanding and accelerating research on other alternative fuels employing this combustion concept.

A fundamental distinction in engine operation lies in the modes of combustion, which also define the main engine technologies [29], as illustrated in Fig. 1. Combustion in ICEs can occur via three modes: (1) premixed flame propagation, typical of spark ignition (SI) engines; (2) non-premixed, mixing-controlled diffusion combustion, which is characteristic of diesel engines; and (3) premixed autoignition, the basis of advanced strategies such as homogeneous charge compression ignition (HCCI). In SI engines, the intended main combustion mode is premixed flame propagation, though some undesirable premixed autoignition

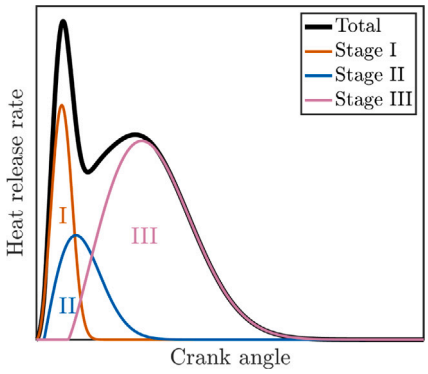

Fig. 2. Dual-fuel conceptual model distinguishing three main combustion stages (based on [17,34])

of the end-gas mixture, typically defined as spark knock, can also occur [30]. This end-gas knock can adversely impact combustion stability and thermal efficiency, while it can risk the mechanical integrity of the engine by introducing pre-ignition and super knock [31,32]. Similarly, while diesel engines also exhibit an initial stage of premixed autoignition depending on the ignition delay (ID), they primarily rely on mixing-controlled combustion. High IDs should be avoided, as they can lead to excessive premixed autoignition, resulting in high peak pressures and pressure rise rates (PRRs) that can damage the engine—a phenomenon commonly referred to as diesel knock [33].

Combustion in PRDF engines is a hybrid between the combustion principles in diesel CI and gasoline SI engines: the premixed autoignition and mixing-controlled combustion of diesel, and the premixed flame propagation and autoignition typical of gasoline engines. To assist the conceptualization of combustion mechanisms in PRDF engines, this study incorporates the theoretical DF model by Karim [17], defined in three overlapping combustion stages, as illustrated in Fig. 2:

- **Stage I** encapsulates the premixed autoignition of pilot diesel, including any entrained LRF.
- **Stage II** defines the combustion deriving from the premixed autoignition of the LRF–air mixture.
- **Stage III** reflects the bulk turbulent flame propagation, along with any remaining diffusion combustion of diesel.

It should be noted that the main deviation from Karim's definition of the three stages lies in the third stage, in which Karim also included premixed autoignition. However, this work redefines the third stage to conceptually separate premixed autoignition from flame propagation in the unburned mixture. This adjustment follows the approach of Ahmad et al. [34], which characterized distinct combustion phases in a methane PRDF single-cylinder engine by combining HRR analysis with optical diagnostics.

The interaction between the pilot diesel's premixed combustion and the subsequent LRF combustion stages is a defining aspect of the multi-stage process in PRDF engines. The Stage I autoignition event governs the amount of LRF that undergoes premixed autoignition near the jets (Stage II), as well as the number and spatial distribution of flame kernels that propagate through the mixture (Stage III). This interplay has a profound influence on overall combustion dynamics and engine performance. Micro-pilot dual-fuel (MPDF) strategies, which minimize the pilot diesel quantity, substantially reduce the influence of Stage I [27]. The resulting ignition energy is often insufficient to robustly initiate Stage II, causing the majority of LRF combustion to shift to Stage III. However, with fewer flame kernels generated, Stage III combustion is weakened and becomes very sensitive to end-gas mixture reactivity properties, such as temperature and equivalence ratio. Low reactivity in the end-gas mixture can lead to slower overall burn rates and increased cycle-to-cycle variability. This deterioration in combustion quality has been experimentally observed by Choi et al. [35] in a methane-fueled MPDF engine, with the slowest combustion rates and highest cyclic variations recorded at the maximum methane energy fraction of 97.86%. Similar trends have been reported by Li et al. [36]. These combustion challenges highlight a fundamental limitation of PRDF strategies at lower load conditions: lower in-cylinder temperatures and leaner mixtures—typical of unthrottled operation—with decreasing loads require the maximum attainable MEF to be drastically reduced to maintain stable combustion [37].

Consequently, although maximizing diesel replacement with LRF is a desirable goal for reducing carbon intensity in DF engines, stable combustion fundamentally depends on maintaining adequate ignition energy from the pilot. As the pilot quantity increases to enhance combustion stability, the system transitions towards a more complex interplay of mechanisms, and the primary challenge shifts from combustion stability to the onset of knock phenomena—namely:

- **Diesel knock**, associated with intensified Stage I combustion.
- **End-gas knock**, related to the induced autoignition in the end-gas region.

PRDF engines often encounter pronounced premixed diesel combustion (Stage I) due to extended IDs caused by air displacement by the LRF. When this coincides with the autoignition of the unburned LRF–air mixture (Stage II), triggered by pressure waves from multiple flame fronts, the combination produces high PRRs that can be detrimental to both engine efficiency and mechanical integrity [38]. To mitigate these challenges, the premixed mixture ignition in the end gas (PREMIER) strategy has been proposed in previous studies, aiming to harness end-gas autoignition and improve PRDF operation [15,39]. This PREMIER approach is analogous to the SACI concept, in which a spark discharge is used to initiate ignition and enable phasing control over the otherwise compression-ignited mixture, thereby offering a lever for combustion phasing in HCCI-type engines [40]. Unlike knocking combustion, the PREMIER strategy enables a controlled premixed autoignition that avoids damaging pressure oscillations [41]. Instead, it aims to initiate ignition around the pilot jets and promote multiple flame propagation, which can improve combustion quality and thermal efficiency [42]. Conversely, if the diesel fraction is further increased to suppress knock and improve combustion control, the influence of the LRF diminishes, resulting in its passive co-combustion role as the combustion process transitions towards two-stage conventional diesel combustion (CDC) [43].

While considerable research has focused on natural gas in the PRDF strategy, significantly less information is available for alternative LRFs such as methanol. This scarcity is even more evident in studies that investigate combustion modes and the interactions between the distinct combustion stages. Methanol, however, introduces two additional parameters that critically influence the dynamics among these stages: its strong cooling effect and chemical inhibition effect [44,45]. Methanol possesses a latent heat of vaporization nearly four times that of diesel. Therefore, considering lower heating values (LHVs) and equal power output, methanol results in a cooling effect nine times greater than that of diesel [46]. Further, introducing methanol with the air in the cylinder limits the production of active radicals at temperatures lower than 1000 K, thus inhibiting diesel ignition. The combination of these effects are expected to significantly influence the ID of the pilot fuel, thereby altering the characteristics of Stage I combustion and its interaction with the subsequent methanol combustion stages. As a result, the already complex PRDF combustion process—and its sensitivity to the LRF fraction—becomes even more pronounced. These factors underline the critical importance of advancing research on methanol combustion in PRDF engine configurations to better understand and promote the use of methanol in marine engines.

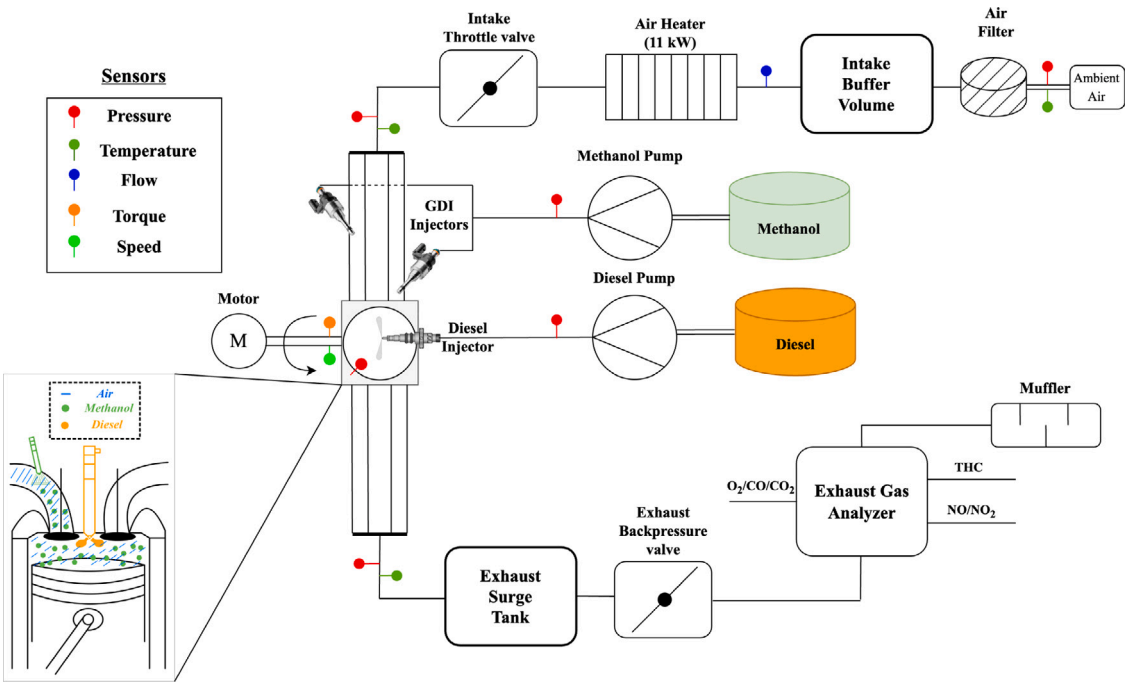

Fig. 3. Schematic diagram of the single-cylinder test setup.

3. Experimental setup

3.1. Apparatus

Experimental investigations were conducted using a single-cylinder research diesel engine featuring a modular design. A schematic of the engine test bed is presented in Fig. 3. The engine features a compression ratio of 14:1, with bore and stroke measuring 170 mm and 180 mm, respectively, resulting in a total displacement of approximately 4.1 L. Key specifications, as well as the properties of the fuels used, are summarized in Table 1.

The diesel fuel system comprises a centrally located injector mounted on the cylinder head, supplied by a mechanical inline pump. The injector nozzle opening pressure is 340 bar. For methanol delivery, a dual-port fuel injection system was implemented to enhance mixture formation controllability. This system utilizes two Bosch HDEV 5.2 injectors, each targeting one of the intake runners. The selection of two Gasoline Direct Injection (GDI) injectors instead of normal PFI injectors was done to improve methanol's atomization and reach high MEFs. A stainless steel plunger pump, with a 150 bar pressure capability, supplies methanol to the injectors. The flow rates of both diesel and methanol were measured using Coriolis mass flow meters, enabling accurate monitoring of fuel consumption and the MEF during the experiments. Surge tanks on both the intake and exhaust sides dampen pressure fluctuations inherent to single-cylinder engine operation. An 11 kWe electric heater is installed in the engine setup to provide additional control over the intake air temperature, a critical impacting factor on methanol evaporation and combustion efficiency.

3.2. Data acquisition and processing

This research focuses on steady-state combustion and performance analysis. Slow-speed data, including intake/exhaust manifold pressure and temperature, mass flow rates, and exhaust gas species concentrations, were acquired using a 10 Hz logger and averaged over a one-minute interval. An uncooled Kistler 6125C piezoelectric pressure transducer, coupled to a charge amplifier, is employed to measure the in-cylinder pressure, which forms the basis for combustion analysis in this study. A crank angle encoder with 0.1 °CA resolution is synchronized to the acquisition system. Pressure signals from 50 consecutive cycles are processed using a first-order Savitzky–Golay filter with 2.7 °CA frame length. This filtering strategy is chosen to avoid over-smoothing, keep the non-physical heat release rate at low levels, and to separate the main combustion stages in both diesel-only (DO) and DF modes [47]. An ensemble-averaged pressure trace was derived from the filtered cycles, serving as the input for the heat release analysis.

3.3. Operating test conditions

This study investigates the two highest load points tested during D2 test cycle experiments on the engine at 1500 rpm, corresponding to torques of 300 N m and 420 N m. These operating points represent gross indicated mean effective pressures (gIMEPs) of approximately 11 and 15 bar, respectively, and serve as the primary load conditions for the analysis. Initial tests were conducted under diesel-only (DO) operation to establish a baseline for comparison, after which methanol was incrementally introduced. Although diesel injection activation was kept constant across all operating conditions, the actual start of injection could fluctuate slightly due to variations in in-cylinder pressure affecting needle valve opening.

Intake conditions during MEF sweeps were kept constant within each sweep but slightly increased relative to DO operation. The intake temperature rose from 298 K in DO operation to 333 K at 300 N m and 323 K at 420 N m under methanol operation. There was an additional controlled increase in charge air temperature beyond 88% to explore the combustion sensitivity to air temperature. Table 2 summarizes the experimental operating points, including the temperature (T_{IVC}) and pressure (p_{IVC}) at inlet valve closure (IVC), which represent the trapped charge boundary conditions at the start of compression for each test. These parameters provide insight into the small variations in thermodynamic conditions across the various cases. The main control parameters assessed in this study are, therefore, load and MEF, with Table 2 providing details regarding the experimental test operating points. To evaluate load effects on combustion characteristics, MEF sweeps were performed at both high-load conditions. At 11 bar gIMEP, MEF was varied from 62% to 86%, while at 15 bar gIMEP, the sweep

Table 1
Engine and fuel specifications.

Parameter	Specification
Engine	
Type	1-cyl 4-stroke CI
Bore x Stroke [mm]	170 × 180
Displacement [L]	4.1
Piston bowl shape	ω
Number of valves	4
Compression Ratio [–]	14:1
Fuels	
Diesel type	EN590
Diesel LHV [MJ/kg]	42.7
Diesel HC ratio	1.88:1
Methanol type	ISO 6583 Grade A
Methanol LHV [MJ/kg]	19.9

ranged from 79% to 93%. The upper and lower limits of the MEF sweeps were determined by elevated cyclic variations and onset of excessive knocking, respectively, with the operational constraints further elaborated in Section 5.

4. Data analysis methodology

This section provides details regarding the methodology followed to analyze combustion based on the in-cylinder pressure data. The analysis, including combustion and performance diagnostics, is developed in the environment of MATLAB and Simulink [48].

4.1. Performance characteristics

The oxygen content of alcohol fuels results in lower LHVs compared to conventional hydrocarbons, with methanol's LHV being approximately half that of diesel fuel. This study employs the MEF metric for quantifying methanol utilization over diesel, defined as:

$$\mathrm{MEF} = \frac{\dot{m}_\mathrm{m} \cdot \mathrm{LHV_m}}{\dot{m}_\mathrm{m} \cdot \mathrm{LHV_m} + \dot{m}_\mathrm{d} \cdot \mathrm{LHV_d}} \cdot 100\% \tag{1}$$

where $\dot{m}$ is the mass flow rate of each fuel, $\mathrm{LHV_i}$ is the lower heating value of the fuel, and subscripts m and d correspond to methanol and diesel fuel, respectively.

The global air excess ratio λ is defined as:

$$\lambda_\mathrm{global} = \frac{\dot{m}_\mathrm{air}}{(\dot{m}_\mathrm{m} + \dot{m}_\mathrm{d}) \cdot (\mathrm{MMF} \cdot \mathrm{AFR_{stoich,m}} + (1 - \mathrm{MMF}) \cdot \mathrm{AFR_{stoich,d}})} \tag{2}$$

where $\dot{m}_\mathrm{air}$ is the mass flow rate of air, and $\mathrm{AFR_{stoich,i}}$ is the stoichiometric air-to-fuel ratio for each fuel.

Combustion efficiency is estimated through an energy balance accounting for exhaust constituents. For DO operation, unburned hydrocarbon (UHC) emissions are treated as carbonaceous compounds using diesel's H/C ratio. For methanol operation, the interpretation of UHC emissions is complicated by the low sensitivity of the Flame Ionization Detector (FID) to oxygenated species such as methanol, as well as its negligible response to formaldehydes (HCHO) [49]. In this study, to estimate combustion efficiency under methanol DF mode, UHCs are assumed to consist predominantly of unburned methanol, rather than significant contributions from formaldehyde or other partial oxidation products [50,51]. In both modes, however, CO emissions are directly measured and converted to energy loss using its LHV. While these approximations in both modes limit the exact specification and quantification of UHC components, they provide consistent comparative analysis across the modes. The combustion efficiency η_comb, therefore, follows:

$$\eta_\mathrm{comb} = \left(1 - \frac{1 + \lambda_\mathrm{global} \cdot \mathrm{AFR_{stoich.}} \cdot \sum_{i=1}^{n_\mathrm{UHC}} y_i^{exh} \cdot \mathrm{LHV_i}}{\mathrm{LHV_{fuel}}}\right) \cdot 100\% \tag{3}$$

where y_i^{exh} is the mass fraction of the defined UHC in the exhaust gases, with the general form of equation deriving from representing exhaust gas flow components based on the fuel by using the terms of air excess ratio λ and $\mathrm{AFR_{stoich}}$ [52]. Gross indicated power forms the basis for performance evaluation:

$$P_\mathrm{gross,ind} = \frac{\int_{\theta=-180}^{\theta=180} p_i(\theta) \cdot dV_i(\theta) \cdot n_\mathrm{eng}}{k \cdot 60} \tag{4}$$

where θ denotes crank angle, p_i and V_i the instantaneous pressure and volume, n_eng the engine speed in rpm, and k the number of revolutions per power cycle. Emission indices, including CO, CO_2, NO, and NO_2 are normalized by gross power output, except for UHC which is quantified in ppm units due to the challenges to determine the composition of UHC emissions with FID. An example for the quantification of the indicated specific emissions is given for nitric oxide:

$$\mathrm{ISNO} = \frac{\dot{m}_\mathrm{NO}}{P_\mathrm{gross,ind}} \tag{5}$$

Cycle-to-cycle variation is quantified through the coefficient of variation (COV) of gross indicated mean effective pressure (gIMEP):

$$\mathrm{COV}_x = \frac{\sigma_x}{\mu_x} \cdot 100\% \tag{6}$$

with μ_x and σ_x representing the mean and standard deviation over N_cycles:

$$\mu_x = \frac{\sum_{i=1}^{N_\mathrm{cycles}} x_i}{N_\mathrm{cycles}} \tag{7}$$

$$\sigma_x = \sqrt{\frac{\sum_{i=1}^{N_\mathrm{cycles}} (x_i - \mu_x)^2}{N_\mathrm{cycles}}} \tag{8}$$

The distribution of fuel energy within the engine cycle is quantified using mean effective pressure (MEP) terms, which provide a normalized basis for comparing energy flows relative to the displaced cylinder volume. The total fuel energy input is expressed as:

$$\mathrm{MEP_{fuel}} = \frac{\dot{m}_\mathrm{fuel} \cdot \mathrm{LHV_{fuel}}}{V_d} \tag{9}$$

where $\mathrm{MEP_{fuel}}$ is the MEP for the fuel energy input, and V_d is the displaced cylinder volume. Combustion losses (CL) are determined based on the estimated combustion efficiency, while heat losses (HL) are calculated using the calibrated heat transfer model evaluated at EVO. The gross indicated mean effective pressure (gIMEP) is obtained directly from the in-cylinder pressure measurements. The exhaust losses (EL) are then determined by closing the energy balance according to:

$$\mathrm{MEP_{EL}} = \mathrm{MEP_{fuel}} - \mathrm{MEP_{CL}} - \mathrm{MEP_{HL}} - \mathrm{IMEP} \tag{10}$$

4.2. Heat release rate

The combustion analysis employs a zero-dimensional, single-zone thermodynamic model based on the first law of thermodynamics for closed systems during the closed in-cylinder process period (IVC to EVO) [52,53]. Species-specific thermodynamic properties are computed via temperature-dependent power series [54]. Trapped conditions at IVC were determined through the isentropic expansion assumption of residual gases from EVO to EVC ($\gamma = 1.32$), assuming negligible valve overlap [55,56]. The temperature of intake charge incorporated heat pickup from valves/ports, subsequently mixing with the hot residual gases. The apparent heat release rate (aHRR) is derived from energy conservation principles:

$$\mathrm{aHRR} = \dot{Q}_\mathrm{comb,app}(\theta) = m \cdot c_v(\theta) \cdot \frac{dT(\theta)}{d\theta} + p(\theta) \cdot \frac{dV(\theta)}{d\theta} \tag{11}$$

where m represents the trapped in-cylinder mass, c_v the specific heat at constant volume, T the bulk gas temperature (calculated via ideal

Table 2
Experimental operating points.

Mode	gIMEP [bar]	Diesel flow [grams/cycle]	Methanol flow [grams/cycle]	MEF [%]	Air Excess ratio [–]	T_{IVC} [K]	p_{IVC} [bar]
Diesel only	2.83	0.06	0	0	6.04	326	1.37
	11.09	0.22	0	0	2.85	348	2.38
	14.95	0.30	0	0	2.59	348	2.90
Methanol DF [11 bar]	10.64	0.087	0.284	62	2.35	346	1.90
	10.13	0.079	0.284	64	2.45	346	1.91
	10.55	0.078	0.301	66	2.37	342	1.89
	10.50	0.070	0.320	69	2.37	339	1.88
	10.66	0.063	0.344	73	2.33	337	1.87
	10.57	0.057	0.364	76	2.29	337	1.87
	10.54	0.050	0.390	79	2.26	332	1.85
	10.74	0.045	0.409	82	2.22	329	1.84
	10.66	0.040	0.425	84	2.20	328	1.84
	10.71	0.035	0.451	86	2.14	325	1.83
Methanol DF [15 bar]	15.18	0.071	0.535	79	2.58	329	2.90
	15.24	0.067	0.547	80	2.56	330	2.90
	15.23	0.063	0.554	81	2.56	329	2.89
	15.15	0.060	0.564	82	2.56	327	2.88
	15.16	0.055	0.574	84	2.56	328	2.88
	15.17	0.048	0.598	86	2.52	325	2.85
	15.13	0.040	0.626	88	2.48	323	2.84
	15.08	0.033	0.622	90	2.55	327	2.87
	14.98	0.023	0.595	93	2.72	340	2.95

gas law), p the measured in-cylinder pressure, and V the instantaneous cylinder volume.

The gross heat release rate (gHRR) extends this formulation by incorporating heat transfer losses:

$$\text{gHRR} = \dot{Q}_{\text{comb,gross}}(\theta) = \dot{Q}_{\text{comb,app}} + \dot{Q}_{\text{loss,wall}} \tag{12}$$

where $\dot{Q}_{\text{loss,wall}}$ quantifies convective heat transfer through cylinder boundaries using the Woschni correlation [57]. The heat transfer model was calibrated against the estimates of combustion efficiency [58]. Diesel combustion is assumed to be instantaneous upon injection, producing stoichiometric products. For methanol, full evaporation at IVC is assumed. The crank angle at which x% of the cumulative aHRR is reached, denoted as CAx, is used to characterize different combustion phases. This approach is selected to avoid the uncertainties associated with heat transfer modeling inherent in gHRR calculations.

4.3. Dual-fuel combustion characteristics

To quantify and analyze combustion characteristics in the PRDF concept, this study employs suitable metrics for its unique behavior, moving beyond traditional combustion parameters. A primary objective is quantifying the transition between distinct combustion phases. Li et al. [59] divided the HRR profile into two segments by identifying a tangency point in the HRR signal, which they used to assess the effects of the defined stages in the vibration levels of a methanol-fueled PRDF engine. For combustion phasing analysis, this study adopts metrics validated in optical investigations of PRDF combustion that correlated HRR profile markers with physical combustion transitions, as illustrated by Fig. 4. Following the approach of Ahmad et al. [34], the local maxima of the HRR profile are employed to divide the overall combustion process into:

1. **Delay phase (Ignition delay):** Spanning from start of injection (θ_{SOI}) to the first local maxima (θ_1), i.e., start of combustion (SOC).
2. **Combustion Phase I (Pilot combustion):** Extending from SOC to the second local maxima (θ_2), dominated by diesel premixed autoignition (Stage I).
3. **Combustion Phase II (Methanol combustion):** Covering the interval from (θ_2) to θ_{EOC} (matching CA90), encompassing methanol combustion via autoignition (Stage II) or flame propagation (Stage III).

SOI is defined as the moment when the fuel pressure in the injector line reaches the needle opening threshold, indicating the onset of needle lift and the beginning of fuel injection. Combustion duration (CD) is defined as the interval θ_1-θ_{EOC}. A key distinction from the study of Ahmad et al. on methane PRDF combustion lies in the characteristics of the observed HRR profiles, which reflect differences in the staging of underlying combustion mechanisms. Whereas Ahmad et al.'s optical analysis revealed a clear separation of all combustion stages—producing multi-peak second derivatives—this study consistently observes clear two-peak HRR profiles. This outcome is attributed to the delay and separated combustion of methanol relative to the initial diesel premixed combustion, resulting in significant overlap between the combustion mechanisms associated with methanol [60]. This overlap, which was not observed with the methane PRDF concept, may be attributed to the distinct charge-cooling effect of methanol. Here, the first local maximum remains the mark for diesel premixed autoignition and SOC, while the second signifies methanol combustion initiation—whether through premixed autoignition or flame propagation.

Following the description of the quantitative analysis of combustion characteristics, it is necessary to clarify the terminology to avoid ambiguity, as the terms *combustion stages* and *combustion phases* are used extensively in the discussion of results. As depicted in Fig. 4, the quantitative combustion methodology cannot resolve the three combustion stages defined in Section 2. Therefore, throughout this study, the term *combustion stages* refers to the mode-informed qualitative analysis, while *combustion phases* refers to the two-phase (diesel and methanol) division obtained from the quantitative analysis. In short, combustion phases capture quantitative trends, whereas combustion staging provides complementary qualitative insights into underlying mechanisms that are not clearly distinguished by the quantitative approach.

4.4. Knocking characteristics

This study uses two complementary metrics to assess knocking: the maximum pressure rise rate (PRR_{max}) and the maximum amplitude of pressure oscillations (MAPO), as determined by Eqs. (13) and (14), respectively:

$$\text{PRR} = \max\left(\frac{dp_{\text{filt}}}{d\theta}\right) \tag{13}$$

$$\text{MAPO} = \max\left(\left|p_{\text{filt,freq}}\right|_{\theta_0+w}^{\theta_0}\right) \tag{14}$$

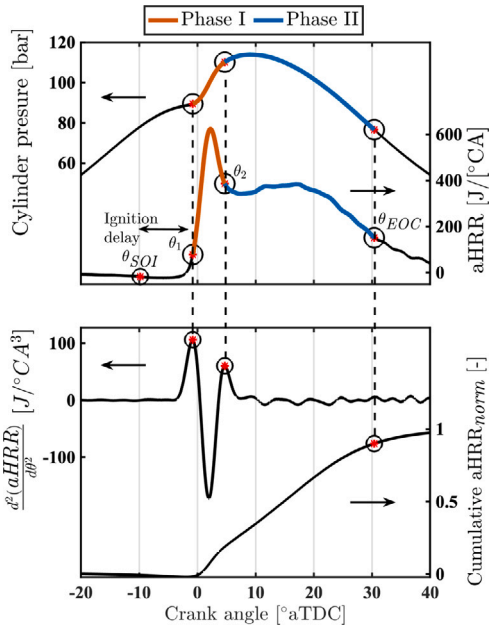

Fig. 4. Combustion phasing methodology.

where p is the raw pressure, p_{filt} the filtered pressure with Savitzky–Golay filter, $p_{\text{filt,freq}}$ is the high-pass filtered pressure, θ is the crank angle, and w is the filtering crank angle window. PRR_{max}, calculated as the steepest slope of the in-cylinder pressure trace, serves as an indicator of the severity of rapid premixed combustion of the pilot diesel (diesel knock), which is particularly relevant given methanol's sensitivity to IDs. MAPO is employed to quantify the high-frequency pressure fluctuations associated with knock phenomena, including both diesel and end-gas knock. For its calculation, the in-cylinder pressure signal is filtered using a bandpass filter (p_{filt}), with a frequency range of 2 to 20 kHz. The lower cutoff at 2 kHz accounts for the reduced natural acoustic frequencies in large-bore engines, while the upper limit of 20 kHz is well below the measurement system's Nyquist frequency (45 kHz), ensuring accurate signal representation without introducing high-frequency noise [61,62]. The crank angle window for knock analysis (w) begins at the start of injection and spans 60 °CA.

Recognizing that pressure oscillations can originate from both rapid premixed diesel combustion and end-gas autoignition [33,63], MAPO is quantified separately for the two main combustion Phases I and II. This approach allows for partial distinction between pressure fluctuations arising from the initial diesel-driven combustion and those associated with methanol combustion in the second stage during the bulk flame propagation. This methodology reflects the dual-knock nature inherent to PRDF operation, as discussed in Section 2. As this study does not include dedicated knock limit testing, these metrics are used to compare relative knock intensity between operating points, thereby supporting the broader analysis of combustion modes.

5. Results and discussions

5.1. Premixed dual-fuel operation with methanol

Before examining the effects of methanol addition on the behavior of the diesel engine under PRDF strategy, it is beneficial for the analysis to first compare DO operation—at both minimal and full fueling rates—with DF operation at a representative MEF. This approach enables a clearer distinction between the primary effects of methanol addition on combustion behavior and conventional diesel operation, as well as the main differences between DO and methanol PRDF operation.

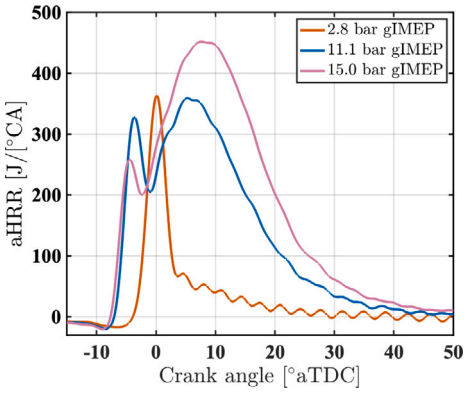

Fig. 5. Single- to double-peak HRR profiles in diesel-only mode.

5.1.1. Methanol influence on diesel's combustion dynamics

At low loads, operation with a minimal amount of diesel results in combustion dominated by a single premixed autoignition phase. As the diesel quantity increases with higher loads, combustion transitions to a two-stage process, as illustrated in Fig. 5. The combination of larger diesel quantities—requiring longer injection durations—and potentially shorter IDs due to a higher thermal state of the combustion chamber components and increased cylinder pressure during injection results in a reduced premixed phase magnitude. This leads to the majority of diesel fuel combusting during the subsequent diffusion phase. In DF operation at high loads and high MEF, the combustion behavior of diesel is expected to closely resemble that observed in the low diesel quantity case (2.8 bar gIMEP), with the addition of methanol modifying the process. To clearly illustrate this effect, Fig. 6 compares heat release profiles for DO and two DF cases, all employing the same pilot diesel quantity of approximately 63 mg/cycle.

For the lower methanol quantity case (a), the introduction of methanol extends the ID by about 1.8 °CA, resulting in a more intense premixed combustion phase. This is reflected in the maximum HRR (HRR_{max}), which nearly doubles from 363 J/°CA to 693 J/°CA. In the higher methanol quantity case (b), although a similar combustion pattern is observed, the ID extension is somewhat shorter—around 1.1 °CA—despite the greater cooling effect expected from the increased methanol mass. This counterintuitive result can be attributed to the higher pressures and global air excess ratio at the higher load (increasing from 2.33 to 2.56), which enhance shear forces on the pilot jet, as well as the higher thermal states of chamber components at higher loads, ultimately improving atomization of the pilot diesel.

Despite the shorter ID in the higher methanol case, the magnitude of the first premixed combustion phase is slightly greater, with HRR_{max} reaching approximately 728 J/°CA. This is due to the larger amount of methanol that is expected to co-combust with pilot diesel, either entrained or simultaneously in the vicinity of the flame, which enhances the energy released in the initial combustion stage. Additionally, in both DF cases, the extended ID relative to DO operation allows for more thorough mixing of diesel with air, promoting combustion under less fuel-rich conditions. Consequently, the majority of diesel fuel is expected to complete its energy release by the end of the first combustion stage [34], as indicated by the black dashed line. These combined effects lead to an intensified first premixed combustion stage, as highlighted by the red shaded region. Quantitatively, methanol addition increases the heat released in the first phase by 100% and 111% in the two DF cases compared to DO, respectively. Notably, the influence of methanol on the pilot's premixed diesel stage in the PRDF concept is substantially more pronounced than that observed with other LRFs, such as natural gas, which typically do not induce such significant changes in the ID of diesel [21].

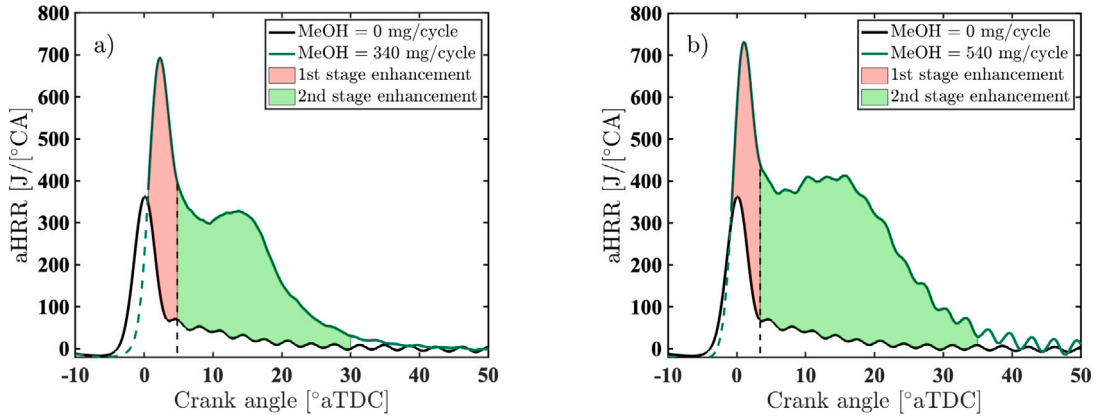

(a) MEF = 72% at 10.7 bar gIMEP **(b)** MEF = 80% at 15.2 bar gIMEP

Fig. 6. Diesel-only to dual-fuel mode operation under the same amount of pilot diesel.

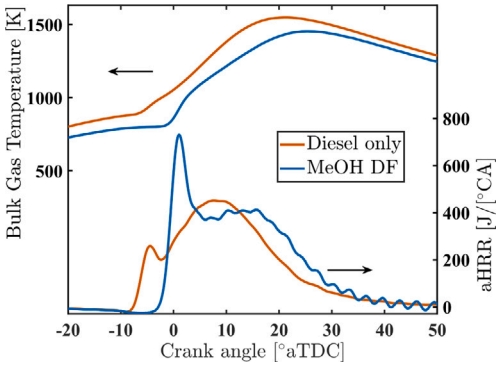

Fig. 7. Comparison of bulk gas temperature and HRR between DO and methanol DF combustion at 15 bar gIMEP.

5.1.2. Diesel-only to methanol premixed dual-fuel operation

The analysis now shifts to a direct comparison between methanol DF and DO operation at the same load, to clearly distinguish the principal characteristics of a diesel engine under methanol operation. Fig. 7 presents the HRR profiles and bulk gas temperatures for both DO and methanol DF cases at 15 bar gIMEP load. Under DO operation, the combination of elevated thermodynamic conditions and higher injection pressures—required to deliver the necessary diesel quantity—results in the shortest IDs observed across the tested load range. This leads to a relatively weak premixed diesel combustion phase, with the majority of fuel burning during the subsequent mixing-controlled stage. In contrast, the introduction of methanol under the DF mode displaces a portion of the intake air and cools the cylinder charge, resulting in an ID increase from 4.4 °CA in the DO case to 9.3 °CA. This prolonged ID enhances the premixed combustion stage, increasing the fraction of total fuel burned in this phase from 10% to 23%.

Comparing the second combustion stages, flame propagation in the methanol DF case proceeds more rapidly than the diffusion phase in DO operation, with durations of 22.2 °CA and 26.6 °CA, respectively. As a result, the overall combustion duration is reduced under methanol operation (27.7 °CA) compared to DO (31.9 °CA). However, this metric does not fully account for the longer ID observed in the methanol case, and thus does not completely capture the shift in combustion phasing. Indeed, the phasing itself is more advanced in the DO case, with the center of heat release (CA50) occurring at 9.6 °CA aTDC compared to 11.8 °CA aTDC for methanol DF operation. Despite the more pronounced and faster premixed combustion stage in the methanol DF case, DO operation yields higher bulk gas temperatures through the combustion window.

The intensified premixed autoignition in the methanol DF mode results in significantly higher pressure rise rates (PRRs). Fig. 8 illustrates the differences in cyclic in-cylinder pressures, including the high-frequency variations revealed by bandpass filtering. The stronger premixed phase in the DF case leads to substantially higher PRRs for each individual cycle, with PRR_{max} nearly doubling from 4.24 bar/°CA in DO to 7.22 bar/°CA in DF operation. The MAPO metric further highlights the highly fluctuating pressure signal characteristic of methanol DF combustion, increasing from 3.4 bar in DO to 9.6 bar in DF operation. Note that the maximum values of the knocking metrics represent the highest values observed across the 50 consecutive cycles recorded for each operating point. Transitioning from DO to methanol DF operation thus produces a significant rise in both PRR_{max} and MAPO, underscoring a greater propensity for combustion knock and less stable combustion. Both rapid premixed diesel combustion and end-gas autoignition contribute to the observed pressure oscillations, resulting in more intense high-pressure waves and stronger knock-like events. This trend towards elevated combustion instability under methanol operation is also reflected in the increased COV_{gIMEP}, which rises from 0.6% in DO to 2.5% in DF mode. The heightened instability underscores the sensitivity of DF operation to abnormal combustion phenomena, highlighting the critical importance of controlling parameters such as ignition timing and air excess ratio to maintain stable engine performance.

A comprehensive evaluation of engine performance between DO and methanol DF operation requires quantifying how the input fuel energy is distributed among useful work and various loss mechanisms. The Sankey diagrams in Fig. 9 illustrate the energy balance for both modes at high-load. Despite both cases achieving similar work output (approximately 15 bar gIMEP), the total fuel energy input is notably higher—by about 12%—in methanol DF operation. This increased requirement arises from the inherent challenges of the methanol PRDF concept, primarily reflected in lower combustion efficiency. Three main factors contribute to this efficiency gap: (1) lower specific heat ratios, in-cylinder temperatures, and leaner mixtures, which weaken flame propagation (mirroring issues in lean SI engines), (2) potential wall wetting effects that can cause methanol to adhere to cylinder surfaces and crevices, and (3) absorption of methanol into oil layers. In this experimental campaign, the latter two factors are considered negligible, as high injection pressures promote effective methanol atomization and evaporation, and lube oil analysis revealed nil methanol contamination below the detection limit of the measurement device. Consequently, the dominant cause of combustion inefficiency is attributed to the relatively low in-cylinder temperatures and high air excess ratios ($\lambda = 2.6$ in this reference case), resulting in 11.8% combustion losses under methanol DF operation.

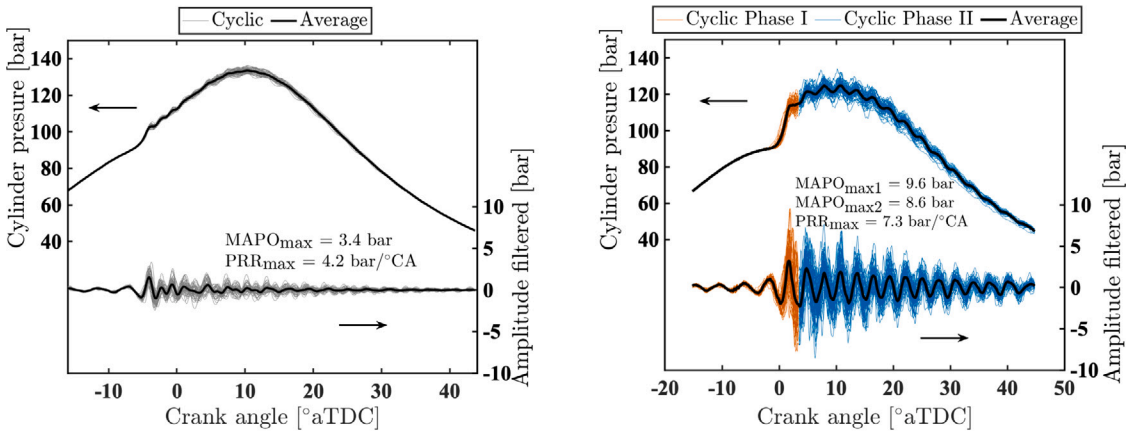

(a) DO at 15.0 bar gIMEP **(b)** DF with MEF = 80% at 15.2 bar gIMEP

Fig. 8. In-cylinder pressure signal along with its bandpass filtered pressure for DO and methanol DF modes at high-load.

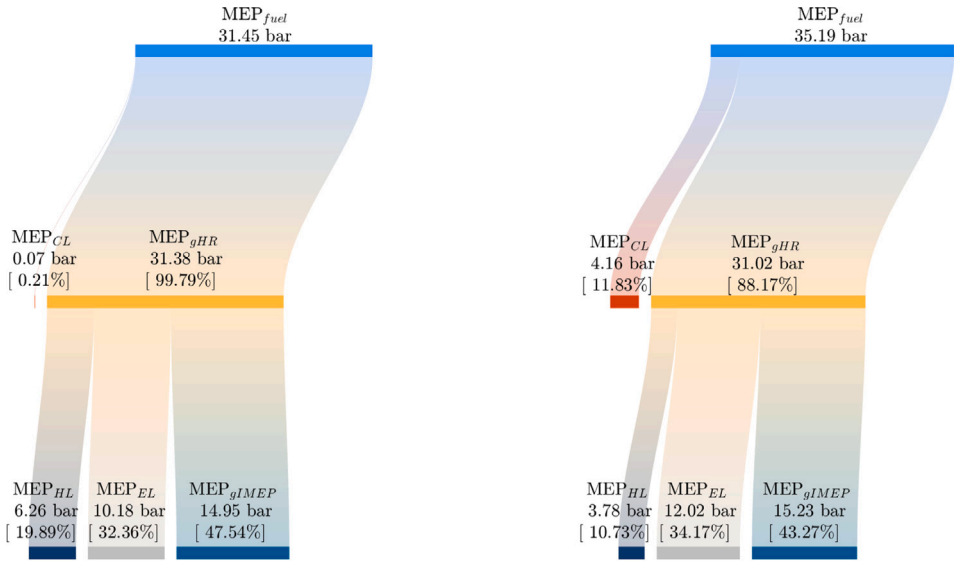

(a) DO at 15.0 bar gIMEP **(b)** DF with MEF = 80% at 15.2 bar gIMEP

Fig. 9. Energy balance using the Sankey diagram for DO and methanol DF operation at high-load.

Interestingly, while the gross heat release is comparable between the two cases, methanol DF operation delivers slightly more work to the piston, despite less favorable combustion phasing compared to DO. This highlights methanol's potential to improve heat efficiency in diesel engines by significantly reducing heat transfer losses, while the slightly decreased thermodynamic efficiency can be further enhanced by advancing combustion phasing through boundary condition adjustments [64]. Ultimately, methanol DF operation fundamentally reconfigures the energy balance within this engine, altering the distribution of input fuel energy. Overall, the gain in the sum of heat and thermodynamic efficiencies—reflecting improved conversion of released fuel energy into piston work—underscores the promise of high-efficiency methanol operation in PRDF engines.

The transition from DO to methanol DF operation also leads to pronounced changes in the diesel engine's emissions profile, as summarized in the comparative bar chart of Fig. 10. As anticipated from the increased combustion inefficiency, methanol DF operation is characterized by a substantial increase in both CO and UHC emissions relative to DO operation. Specifically for this comparative case, CO emissions rise from 0.2 g/kWh to 15.9 g/kWh, while UHC increases from 98 ppm to 4868 ppm. As both emissions are indicators of low combustion efficiency, this trend clearly demonstrates the bottleneck of the PRDF concept being poorer combustion performance.

In contrast, methanol DF mode yields a clear reduction in $ISCO_2$ emissions, decreasing from 554 g/kWh in DO mode to 479 g/kWh under DF operation. While a reduction in CO_2 emissions was expected due to methanol's higher hydrogen-to-carbon ratio compared to diesel, the observed decrease of approximately 13.5% exceeds what would be anticipated solely from this ratio. To isolate the effect of the hydrogen-to-carbon ratio, an estimated perfect combustion in methanol DF operation would yield around 534 g/kWh, corresponding to a reduction of approximately 6%. The greater observed decrease in CO_2 emissions is also influenced by the concurrent increase in CO and UHC, as a fraction of the fuel's carbon remains partially oxidized and is emitted as CO or UHC rather than fully converted to CO_2.

A notable benefit of methanol use is the marked decrease in NO_x emissions. The combination of methanol's charge cooling effect and the more homogeneous combustion environment it fosters contribute to lower peak combustion temperatures, thereby suppressing thermal NO_x formation [65]. In the present study, NO_x emissions are reduced

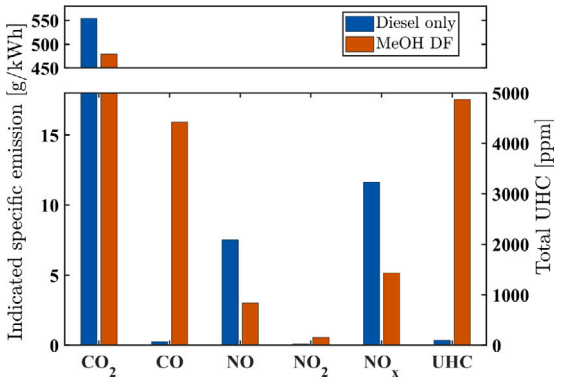

Fig. 10. Comparison of emissions characteristics between DO and methanol DF operation at high-load.

from 11.6 g/kWh in DO operation to 5.2 g/kWh in the DF case. However, since combustion phasing is also expected to influence NO_x formation, the observed decrease cannot be attributed solely to changes in combustion regimes with methanol. A clearer comparison would require adjusting boundary conditions to align combustion phasing more closely with DO operation. Further, the decrease in total NO_x is accompanied by an increase in NO_2 emissions, which rise from 0.1 g/kWh to 0.55 g/kWh. Note that NO_x emissions are quantified based on the molecular weight of NO_2, which explains the discrepancies when comparing the sum of NO and NO_2 to the total reported NO_x values.

The observed increase in NO_2 emissions under methanol PRDF operation has also been reported in previous experimental studies and its interpretation requires insights from mechanistic investigations on NO_2 formation [15,66]. To decouple the effect of methanol's cooling effect from the inherent PRDF combustion behavior, it is interesting to explore the trends with another LRF. Li et al. [67] performed a numerical analysis on a natural gas PRDF engine and found that most NO_2 forms during late post-combustion oxidation of the remaining premixed fuel–air mixture. This occurs predominantly in the end-gas region of the squish area, where local conditions favor low temperature reactions and the abundance of HO_2 radicals promotes the conversion of NO to NO_2 through the $NO + HO_2 \longrightarrow NO_2 + OH$ pathway [68]. The cooling effect of methanol is expected to enhance these low temperature regions, thereby further intensifying NO_2 formation relative to other LRFs.

Overall, the shift to methanol PRDF operation fundamentally alters the emission landscape of the diesel engine. Although this transition offers a reduction in CO_2 and NO_x emissions, it presents a clear trade-off in the form of increased CO, UHC, and NO_2. The wide high-MEF sweeps—including the points compared with DO—are used diagnostically to reveal knock and combustion deterioration challenges, rather than defining applied setpoints. A viable concept will select MEF within an application-specific region that balances knock propensity, desired diesel displacement, NO_x levels, and overall efficiency. These observations reinforce the need to optimize combustion control to utilize the benefits of methanol operation while minimizing its drawbacks. In practice, this may lead to compromises on the maximum MEFs so that gains in emissions, i.e., lower global warming impact, are not offset by excessive efficiency penalties. Accordingly, managing boundary conditions, such as pilot injection timing and air excess ratio, will be central to enabling smooth transitions from DO to methanol PRDF and to robust transient and steady-state operation.

5.2. Combustion mode analysis in methanol dual-fuel mode

The combustion dynamics in PRDF engines are governed by the interplay of multiple mechanisms, resulting in distinct HRR profiles. This complex behavior, inherent to the PRDF strategy regardless of fuel, is further influenced by variations in fuel properties (e.g., methanol's chemical and thermophysical properties) and operating conditions (e.g., load or speed), which dictate the evolution of combustion phasing and heat release characteristics. This subsection develops a systematic analysis of combustion modes in methanol PRDF, integrating both qualitative observations and quantitative assessments, to elucidate the underlying combustion mechanisms and their trends.

5.2.1. Qualitative evaluation

Li et al. [36] identified three primary HRR profiles (h-, m-, and n-shape) in a natural gas PRDF engine at low loads and discussed their distinct combustion processes. Similarly, Lee et al. [69] reported analogous profiles through different operating boundary conditions in gasoline PRDF combustion. For instance, the h-shape profile observed by Li et al. at high natural gas ratios featured a strong premixed combustion stage followed by attenuated flame propagation, whereas Lee et al.'s Mode 1 of a similar shape occurred at low gasoline ratios exhibiting conventional diesel-like characteristics. A core contribution of this study is to expand this qualitative approach, apply it to methanol PRDF data, and ultimately offer a systematic characterization framework for HRR profile morphologies.

In conventional diesel operation, HRR profiles transition from single- to double-peak patterns as load increases, as seen in Fig. 5. Low loads exhibit dominant premixed combustion with a minimal diffusion phase, while higher loads with increasing fuel mass intensify mixing-controlled combustion, yielding a distinct secondary peak. Transitioning to methanol PRDF operation is expected to fundamentally alter this behavior. At very low MEFs, methanol combusts passively during the diesel diffusion phase, thus retaining conventional diesel combustion characteristics, i.e., non-premixed diffusion combustion dominance. As MEF increases, methanol increasingly influences the in-cylinder processes by: (1) extending ID due to its charge-cooling effect, which strengthens the pilot combustion (Stage I), and (2) weakening the diesel diffusion phase as more diesel is consumed in Stage I and a greater portion is replaced by methanol, which primarily combusts via premixed flame propagation (Stage III). Under the lean conditions typical of diesel engines, premixed autoignition of methanol becomes difficult. During this MEF increase, these effects eventually reach critical points: (1) the prolonged ID leads to excessive PRR, risking mechanical integrity and degrading combustion stability, and (2) the reduced augmentation of methanol combustion by diesel diffusion, combined with very lean methanol–air mixtures, further deteriorates combustion stability and reduces combustion efficiency, resulting in high levels of UHC and CO emissions. This combination of mechanical (Diesel knock) and emissions-related (poor combustion) challenges requires imposing limits on MEF to prevent excessive component stresses and to control the emission of methanol and formaldehydes. This limits the MEF to below an average of 50% for most loads in this study, consistent with the findings of Stenzel et al. [26].

Notably, this experimental study identified two distinct MEF operational regions rather than the commonly reported single knock-limited range. Beyond the initial limited window, higher MEFs can re-stabilize combustion and improve efficiency by enriching the methanol–air mixture and enhancing Stage II/III, while inhibiting further enhancement of Stage I by reducing diesel's contribution. This region is restricted by diesel and primarily end-gas knocking at the lower bound, while it is ultimately bounded at the upper end by renewed instability and poor combustion efficiency, as diesel ignition energy becomes insufficient and combustion phasing is delayed extensively. Therefore, the upper and lower MEF limits are determined by different instability mechanisms rather than knock alone, with Fig. 11 qualitatively illustrating these ranges across the MEF sweeps. The subsequent analysis focuses on the high-MEF region.

This research assesses the combustion profiles across the operating points explored in this experiment, i.e., the two high-load MEF sweeps, 11 bar gIMEP and 15 bar gIMEP. Analysis of heat release profiles

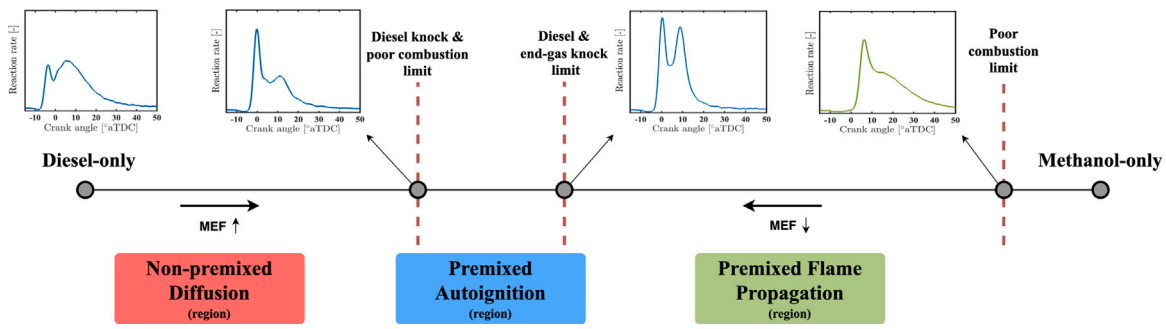

Fig. 11. MEF operational regions in high-load methanol PRDF operation.

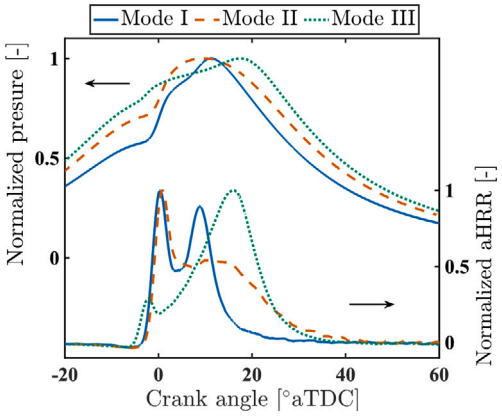

Fig. 12. Defined combustion modes across operating points.

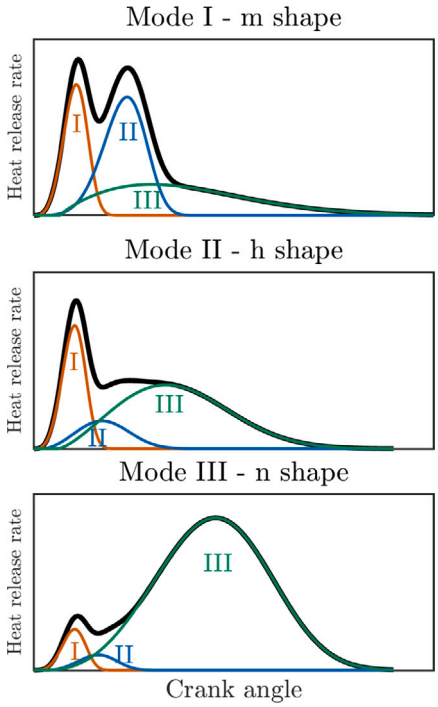

Fig. 13. Conceptual model for the three defined combustion modes.

revealed and defined three distinct combustion modes (I–III) based on their unique HRR shapes, and thus the underlying combustion mechanisms. Fig. 12 illustrates the profiles of HRR and pressure across the defined combustion modes. These modes are classified based on their dominant combustion mechanism, building upon characterization systems [36,60,69] and several optical experimental studies with the PRDF concept [21,34,35,60].

Combustion **Mode I** emerged at the lowest MEF boundary (62%) during the 11 bar gIMEP operation, exhibiting an m-shaped HRR profile with two distinct peaks of comparable magnitude and duration. This peak similarity indicates a common combustion mechanism: premixed autoignition, consistent with the knocking-restricted lower MEF limit. The reduced knocking intensity—compared to levels below the operational threshold—stems from phased separation of both fuels' autoignition event due to delayed methanol–air combustion phasing [60]. This dual-peak profile and the absence of a single-peak HCCI-like profile may also be attributed to the highly lean methanol–air mixtures across the MEF sweeps in this experimental campaign. Optical studies have demonstrated that leaner mixtures tend to reduce the overlap between the premixed autoignition stages of the LRF and diesel [34]. Analogous profiles have been observed in prior PRDF experiments with methanol [65,70], as well as with gasoline [69] and natural gas [36,71]. Fig. 13 illustrates this mode within the conceptual DF framework from Section 2, showcasing the Stages I and II as the dominant heat release mechanisms.

At elevated MEFs, methanol's intensified cooling effect further suppresses premixed autoignition, maintaining a pronounced premixed diesel combustion Stage I despite reduced diesel quantities, while attenuating the secondary combustion phase. The sustained premixed phase arises from prolonged ID, which increases diesel participation in initial combustion and entrained methanol. Conversely, the weakened secondary phase results from the lower reactivity of methanol due to lower temperatures resulting in increased heat release via premixed flame propagation—a comparatively slower mechanism than autoignition. These dynamics define Combustion **Mode II**, exhibiting an h-shaped dual-peak HRR profile with a sharp initial peak and attenuated secondary phase. While premixed Stage I resembles that of Mode I, Stage II is substantially weakened, shifting heat release towards Stage III as depicted in Fig. 13. This mode appeared at all MEFs except the lowest under the 11 bar gIMEP load conditions and low-to-intermediate MEFs at 15 bar gIMEP load.

Conversely, high-load operation at peak MEFs (90%–93%) produced Combustion **Mode III**, exhibiting an n-shaped profile with a dominant second peak. Minimal pilot quantities and IDs diminished premixed diesel autoignition (Stage I), while turbulent flame propagation (Stage III) dominated heat release—aligning with MPDF strategies [39], as depicted in Fig. 13. Reaching high MEFs at high loads required enhancing charge reactivity to promote faster flame propagation and stabilize combustion. This was achieved by increasing intake air temperature, which shortened the pilot diesel ignition delay and improved combustion phasing, while methanol's cooling effect and knock resistance enabled knock-free flame propagation. To avoid confusion, this morphology fundamentally differs from n-shapes reported by Li et al. [36] and Lee et al. [69], which reflect HCCI-like autoignition rather than flame propagation dominance.

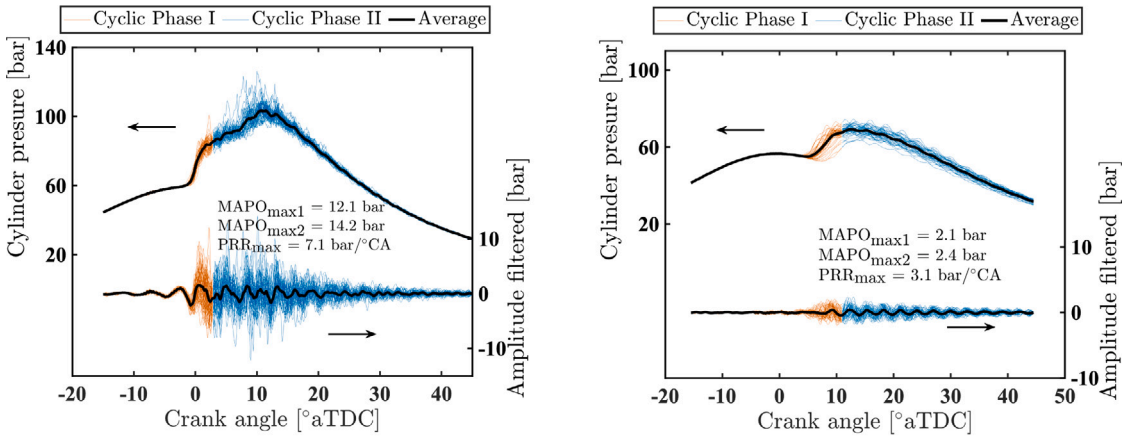

(a) Combustion mode I (MEF 62% at 11 bar gIMEP)

(b) Combustion mode II (MEF 86% at 11 bar gIMEP)

Fig. 14. In-cylinder pressure signal along with its bandpass filtered pressure for combustion Mode I and II at 11 bar gIMEP.

The hypothesis that the attenuated combustion Phase II observed in Mode II arises from a transition in dominant combustion mechanism—from premixed autoignition (Stage II) to flame propagation (Stage III)—can be substantiated by knocking intensity analysis. Fig. 14 displays both raw and bandpass-filtered in-cylinder pressure traces at 11 bar gIMEP for operating points representative of Mode I (62% MEF) and Mode II (86% MEF). The pressure trace analysis demonstrates that Mode I exhibits substantially more persistent and intense pressure oscillations—indicative of knock—compared to Mode II. In the Mode II case, a minor premixed autoignition likely occurs near the jets, corresponding to the weakened Stage II in Fig. 13. By contrast, Mode I exhibits a stronger Stage II, anticipated to originate near the jets and gradually develop into bulk premixed autoignition [72]. This aligns Mode I more closely with the PREMIER combustion strategy commonly used to promotes higher reactivity and controlled end-gas premixed autoignition. Quantitatively, the MAPO in Phase I reaches 12.1 bar at 62% MEF, in clear contrast to 2.1 bar at 86% MEF. For Phase II, this difference persists, with MAPO maxima of 14.2 bar and 2.4 bar, respectively. These pronounced differences confirm that knocking is considerably more significant in Mode I. The greater magnitude of premixed autoignition in Phase I at lower MEF (PRRmax of 7.7 bar/°CA versus 2.95 bar/°CA at the highest MEF) induces stronger in-cylinder pressure fluctuations, which may also propagate and intensify MAPO levels in the subsequent combustion Phase II. The sustained and even increasing pressure fluctuations that extend beyond the end of Phase I further showcase the presence of elevated end-gas autoignition reactivity in Mode I.

5.2.2. Quantitative evaluation

Qualitative analysis of heat release profiles in methanol PRDF combustion revealed distinct morphologies corresponding to varying combustion dynamics. To complement this phenomenological assessment, quantitative characterization of HRR profile evolution is essential for robust combustion mode classification. Comparable approaches have been employed in other studies, ranging from quantifying symmetry and magnitude ratios in a natural gas PRDF engine [36] to tracking the transition from a two- to a single-stage heat release profile in a diesel-ethanol RCCI engine [73].

This study introduces two metrics to systematically characterize HRR profiles in methanol PRDF combustion: the **Combustion Mechanism Index (CMI)** and the **Phase Magnitude Ratio (PMR)**. The CMI quantifies the fraction of the duration from SOC to the peak of Phase I relative to the overall combustion duration:

$$\mathrm{CMI} = \frac{\mathrm{CA}_{\mathrm{PHRR1}} - \mathrm{CA}_{\mathrm{SOC}}}{\mathrm{CA}_{\mathrm{EOC}} - \mathrm{CA}_{\mathrm{SOC}}} \cdot 100\% \tag{15}$$

where $\mathrm{CA}_{\mathrm{PHRR1}}$, $\mathrm{CA}_{\mathrm{SOC}}$, $\mathrm{CA}_{\mathrm{EOC}}$ represent crank angles of the first peak heat release rate, start of combustion, and end of combustion, respectively. Since the first phase in PRDF engines always occurs via premixed autoignition, the CMI expresses the extent to which premixed autoignition dominates the subsequent combustion process. Lower CMI values indicate a relatively longer second phase and greater phase separation, whereas higher CMI values suggest more similar mechanisms between the two phases, with a faster second phase and a more homogeneous profile. The PMR characterizes the relative intensity of Phase I to Phase II:

$$\mathrm{PMR} = \frac{\mathrm{PHRR1}}{\mathrm{HRR60}} \cdot 100\% \tag{16}$$

where PHRR1 represents the first peak in HRR and HRR60 denotes HRR at CA60. The metric was initially calculated with HRR50, but CA50 does not correlate very well with Phase II, limiting its ability to represent the second phase. HRR60 consistently aligned with the actual second-phase peak across all operating modes, making it a more representative choice. PMR values above 100% indicate Phase I dominance, whereas values below 100% reflect Phase II dominance.

Fig. 15 illustrates how the proposed metrics capture profile-shaping characteristics across the three combustion modes. Mode I shows the highest CMI (18.7%), reflecting reduced phase separation (I/II) due to similar combustion rates between phases, which also enhances HRR symmetry. Its moderate PMR above 100% (109.0%) indicates comparable peak magnitudes of the two stages. Mode II exhibits a lower CMI (11.6%) as the flame propagation mechanism prolongs Phase II, creating greater temporal separation between diesel (Phase I) and methanol combustion (Phase II). The elevated PMR (180.5%) reflects the h-shaped profile's dominant first peak, in which intense diesel premixed autoignition (Stage I) overshadows the attenuated methanol combustion phase, primarily via Stage III. This transition from autoignition to flame propagation alters both temporal distribution and magnitude balance, as captured by the metrics. Mode III shows the lowest CMI (10.9%) and PMR (27.1%), indicating stronger temporal asymmetry and clear Phase II dominance. The inverse relationship (PMR< 100%) arises when HRR60 exceeds PHRR1, signifying MPDF combustion with flame propagation generating higher HRR than the initial autoignition of the small pilot diesel. This corresponds to the n-shaped profile observed at extreme MEFs and maximum load, which, as it will be discussed later, required increased intake air temperature to make such high-MEF operation feasible.

Mapping HRR profiles with the combined CMI and PMR metrics establishes a quantitative link between profile shape and underlying combustion behavior, offering a systematic method for combustion mode identification. Fig. 16 shows all operating points from this campaign plotted in the CMI-PMR domain, color-coded by combustion

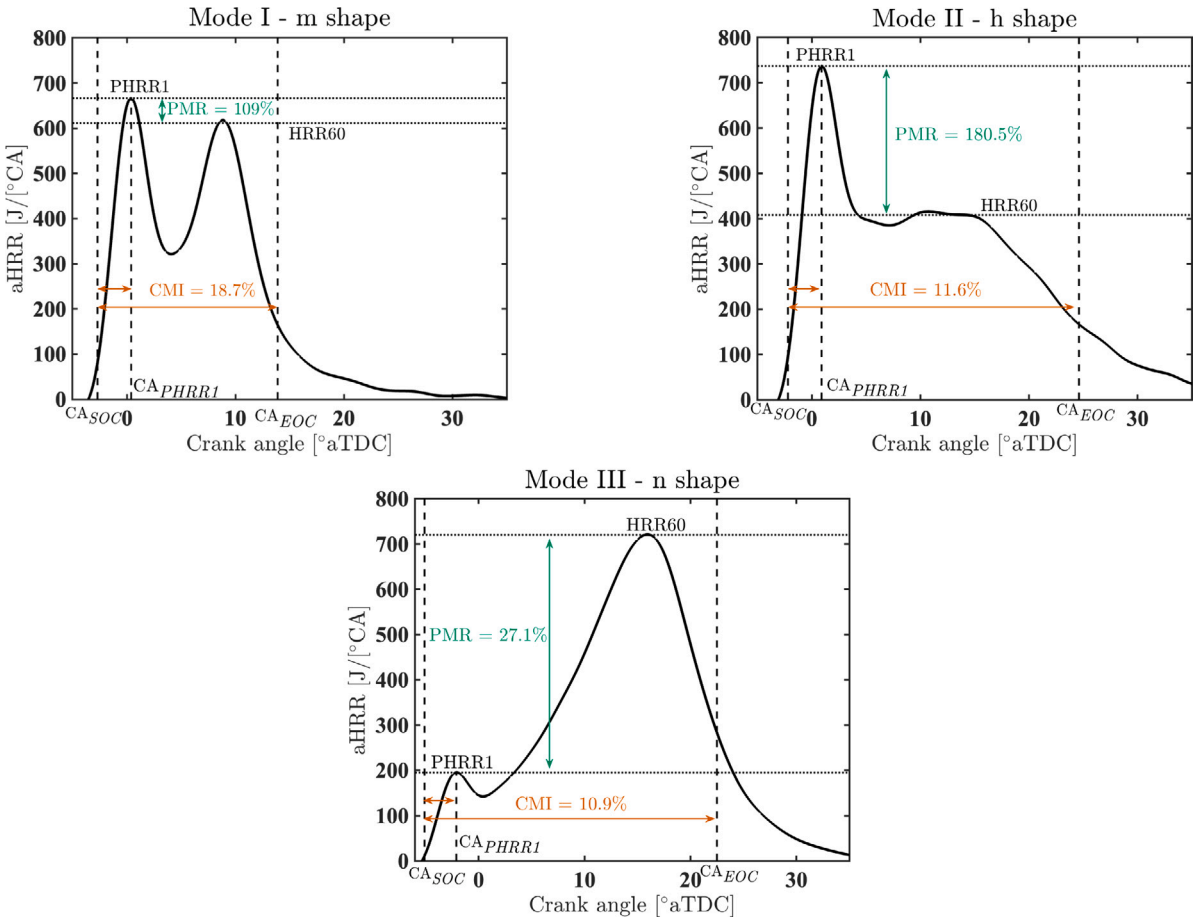

Fig. 15. Shaping characterization methodology using CMI and PMR metrics.

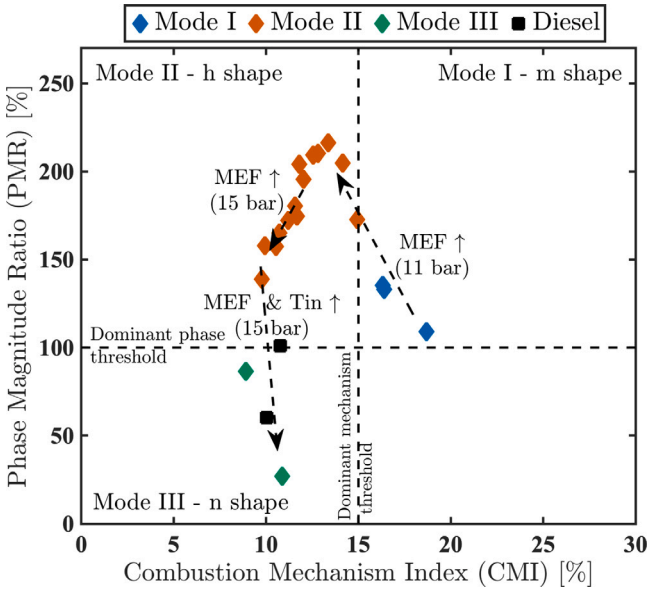

Fig. 16. Heat release profile mapping based on CMI and PMR metrics.

mode, including the DO baseline at 11 and 15 bar gIMEP. Dashed arrows indicate shaping transitions along the two MEF sweeps and the simultaneous intake air temperature increase at the highest load and MEFs.

This visualization reveals four possible regimes, defined by thresholds in the two metrics. The horizontal threshold at PMR = 100% separates first- and second-phase dominance. PMR above 100% indicate a stronger Phase I, typical of Modes I and II, whereas PMR below 100% reflects Phase II dominance, as in Mode III. Concerning DO cases, low-load DO would typically lie above 100% PMR because of the Phase I dominance, while higher load DO shifts below 100% PMR due to a stronger diffusion phase. These profiles resemble the n-shaped Mode III observed in methanol operation. The MEF sweeps demonstrate opposite PMR trends. At 11 bar gIMEP, PMR rises with increasing MEF, as methanol's cooling effect drives the transition from m- to h-shaped profiles, increasing the Phase I to II magnitude gap. At 15 bar gIMEP, however, PMR decreases since Phase I weakens while Phase II remains nearly constant. When PMR falls below 100%, the dominance of methanol flame propagation emerges (Stage III), enabled by the elevated intake temperatures.

The vertical threshold, set at CMI ≈ 15%, further differentiates regimes by combustion mechanism. Higher CMI values indicate more symmetric profiles with phases more evenly distributed between SOC, PHRR1, and EOC, as in Mode I. Low CMI values, approaching 0%, reflect greater temporal separation between combustion phases, typical of flame-propagation-dominated Modes II and III. The 15% threshold was approximately chosen, acknowledging the limits of pressure-based HRR evaluation. More refined thresholds could be derived from optical diagnostics, detailed knock analysis, or chemical kinetics-based modeling.

Within this framework, three quadrants are populated experimentally:

- Quadrant I (CMI > 15%, PMR > 100%): Mode I (m-shape).

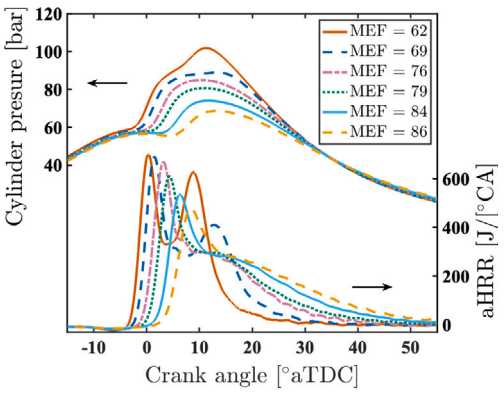

(a) 11 bar gIMEP

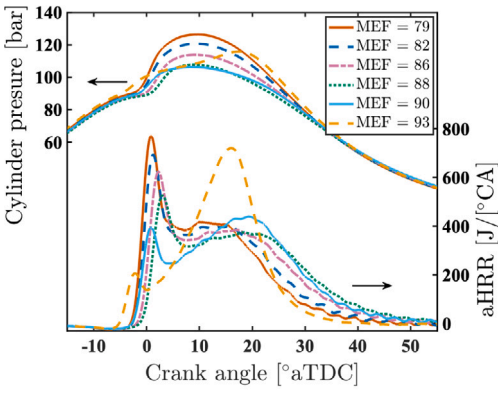

(b) 15 bar gIMEP

Fig. 17. In-cylinder pressure and aHRR across the two MEF sweeps.

- Quadrant II (CMI < 15%, PMR > 100%): Mode II (h-shape).
- Quadrant III (CMI < 15%, PMR < 100%): Mode III (n-shape).

Quadrant IV (CMI > 15%, PMR < 100%), representing strong methanol autoignition similar to Mode I but with Phase II dominance, was not realized experimentally in this study. Such a regime could likely be achieved under higher reactivity conditions. However, these conditions must be carefully controlled, as they drive the engine closer to knock, as seen in the closest case that approached 100% PMR. In theory, CMI exceeding 30% together with PMR near 100% would indicate an RCCI-like homogeneous autoignition regime.

5.3. Impact of MEF sweeps on combustion, performance, and emissions characteristics

Following the direct comparison between DO and methanol DF operation and combustion mode analysis, this subsection systematically explores the effects of varying MEF at the two high-load points (around 11 and 15 bar gIMEP). By examining both load points in parallel, the discussion aims to provide direct insights into load-dependent characteristics together with the methanol effect, due to the influence of different boundary conditions such as air excess ratio and in-cylinder temperatures. Fig. 17 illustrates the effects of varying MEF at the two high-load points tested.

5.3.1. Combustion phasing and duration

At the 11 bar gIMEP load point, the evolution of heat release profile with incremental increases in MEF becomes particularly evident, building on the combustion mode analysis presented earlier. As MEF increases, the characteristic m-shaped profile of combustion Mode I transitions progressively towards the h-shaped profile associated with combustion Mode II. This shift is primarily driven by the enhanced charge cooling effect of methanol, which delays ignition, as reflected in the steady increase in ID from 8.8 °CA to 14.4 °CA across the MEF sweep relative to 5.3 °CA in DO, as shown in Fig. 18. Interestingly, the extended ID does not result in a more pronounced Phase I. Instead, the premixed phase only marginally lengthens—from 5.5 °CA at the minimum MEF to 6.5 °CA at the maximum—and its intensity diminishes, as indicated by a decrease in the HRR_{max} from 685 J/°CA to 476 J/°CA. This attenuation can be attributed to the later phasing of combustion after TDC, which makes the thermodynamic conditions, pressure and temperature, less favorable for methanol autoignition alongside diesel in Stages I/II. The increased displacement of air with higher MEF further deteriorates the mixing quality of diesel and air during the ID period. As a result, the less intense premixed combustion during Phase I leads to a correspondingly weaker and more prolonged Phase II, as the duration of the methanol–air combustion phase increases from 11.1 °CA to 27.6 °CA. Both CA50 and EOC are delayed with increasing MEF, with the combustion duration at the highest MEF being more than twice that at the lowest MEF.

Interestingly, for MEF values below 82%, the combustion duration is actually shorter than in the DO baseline at the same load, despite a longer ID and a slightly more retarded CA50. This effect is primarily due to a more pronounced Phase II, which is significantly shorter than the mixing-controlled second phase in DO operation. For example, at a minimum MEF of 62%, Phase II lasts about 11.1 °CA, compared to 23.3 °CA for the diffusion phase in DO mode. These observations underscore the nuanced sensitivity of combustion phasing metrics in PRDF strategies. Notably, the most advanced CA50 does not always correspond to the fastest overall combustion, as variations in the behavior of the second phase can lead to extended combustion durations. Therefore, it is essential to consider both combustion duration and additional phasing metrics, such as CA60, for a comprehensive evaluation of PRDF combustion and its comparison with DO operation. Additionally, at minimum MEF, all combustion phasing characteristics—including CA50—are more optimal than in the DO case, counterbalancing the overall ignition delay in methanol PRDF operation.

At 15 bar gIMEP, the evolution of the heat release profile reveals a distinctly different trend from that observed at the lower load point of 11 bar gIMEP. As the MEF increases, the initial response mirrors the lower load case; ID becomes longer with combustion phasing gradually deteriorating. However, a critical transition occurs once MEF exceeds 88%. Beyond this point, ID decreases sharply, leading to a more advanced Phase I of combustion—an effect most pronounced at the higher MEFs (90% and 93%). This abrupt change in ignition profoundly impacts the subsequent combustion dynamics. The primary driver of this ignition phenomenon was a targeted adjustment in intake air temperature, from 323 K at MEF below 88% to 333 K and 353 K at 90% and 93% MEF, respectively. This was implemented to briefly assess the stability enhancement at these higher MEFs with an adjustment in such an operating control parameter. The temperature increase improved in-cylinder thermal conditions at the time of diesel injection, gradually advancing combustion phasing and improving efficiency. Consequently, less fuel was required for both methanol and diesel to maintain the target load, resulting in a reduced methanol cooling effect that further supported phasing advancement and a subsequent increase in air excess ratio from 2.48 to a peak of 2.72. These combined boundary condition changes ultimately reduced ID and overall improved combustion performance. While this study focuses on MEF effects under nominally constant boundaries, the observed improvements from this temperature adjustment underscore the value of simple parameter optimization in methanol PRDF engines.

The observed shift in ID at the highest load, deriving from adjustments in boundary conditions, fundamentally changes the subsequent combustion dynamics and results in a clear improvement in overall combustion performance. At 93% MEF, methanol DF operation

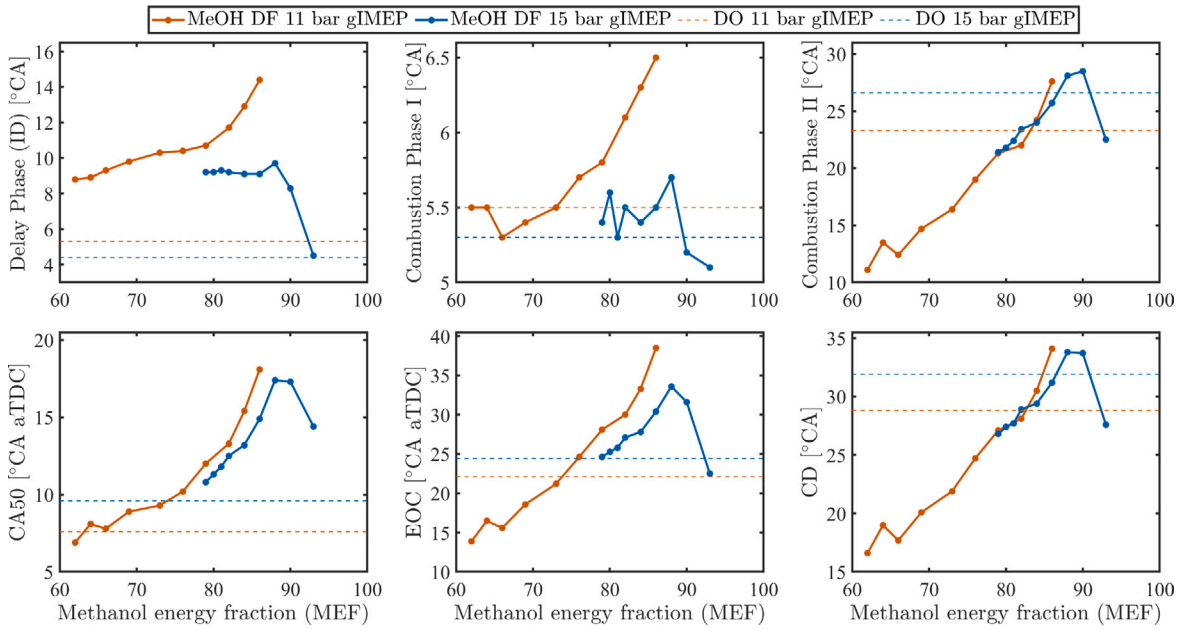

Fig. 18. Effect of MEF on combustion phasing and duration for the two high-load points.

achieves IDs comparable to those of the DO mode, yet with a key distinction in combustion phasing and heat release propagation. Despite similar IDs, CA50 remains more advanced in DO mode, occurring at 9.6 °CA aTDC versus 14.4 °CA aTDC for methanol operation. However, it is in the latter half of the heat release process in which methanol DF distinct combustion mode becomes more evident. In methanol DF conditions with 93% MEF, combustion Phase II is notably faster, with its duration decreasing from 26.6 °CA in DO to 22.5 °CA. This acceleration in the latter combustion phase enables the entire combustion event in methanol operation to finish earlier, as reflected in a more advanced EOC, 22.5 °CA aTDC relative to 24.4 °CA in DO. The changing behavior is attributed to the fundamental difference between the combustion regimes of the two strategies in their second combustion phase. At 93% MEF, methanol DF operation tends towards a MPDF regime, dominated by premixed bulk turbulent flame propagation, whereas the DO case remains characterized by mixing-controlled combustion phase. The formation and development of flame kernels take longer to initiate than the onset of mixing-controlled combustion in DO, resulting in initially slower heat releases in the DF mode. Yet, once these flame kernels are established and a bulk turbulent flame propagation is initiated, combustion rate is higher than that of diffusion-limited combustion under DO, enabling the second combustion phase in methanol DF to overtake the first phase and ultimately produce a shorter total combustion duration, decreasing it to 27.6 °CA from 31.9 °CA under DO.

Comparing the operating points across the MEF sweep reveals how shortening the ID and advancing flame initiation towards TDC fundamentally enhance combustion performance, mirroring the behavior in SI engines. Even though the ignition energy from the pilot jet diminishes at the highest MEF—as evidenced by the reduction in HRR_{max} from 736 J/°CA at 79% MEF to 195 J/°CA at 93% MEF—the advancement of ignition timing creates more favorable thermodynamic conditions near TDC. This better phasing supports more robust flame propagation, underscoring that, in this regime, combustion performance is more sensitive to ignition timing of the pilot fuel than to its absolute energy—a trend also well-aligned with knowledge from SI engines [74,75]. Moreover, the performance of flame propagation observed at a global air excess ratio of 2.72 highlights the strong capability of multi-point pilot-induced flames to sustain efficient combustion under very lean conditions. This stands in contrast to conventional lean-burn SI engines, which typically cannot operate stably at λ greater than 1.6, particularly in large HD applications [76,77].

5.3.2. Combustion stability and engine performance

The intricate balance between combustion phasing, stability, and engine performance is critical in PRDF operations. Advancing combustion closer to TDC is typically desired to maximize thermal efficiency, yet it often escalates knocking propensity, challenging engine stability and its mechanical integrity. Given this interdependency, it is essential to assess a variety of combustion metrics, including peak PRR (PRR_{max}), peak pressure (P_{max}), MAPO, and COV_{gIMEP} to better characterize engine response.

Fig. 19 illustrates how these key indicators vary across the MEF sweeps at both analyzed load points. To provide deeper insights into the combustion process, an additional metric is illustrated: the ratio of the heat released during Phase I to the total heat release (HR_I), offering quantitative information of the relative intensity of the premixed combustion phase. As expected from combustion phasing results, HR_I is more pronounced during methanol DF operation compared to DO due to the increased IDs, except the two highest MEF at 15 bar gIMEP load point. However, the trend of HR_I is decreasing with increasing MEF despite the increased IDs, as it drops from 33.1% to 26.5% and from 25% to 6.2% across the two MEF sweeps of 11 and 15 bar gIMEP load points. This can be attributed to the less favorable thermodynamic conditions when premixed Phase I occurs farther away from TDC, resulting in less methanol combusting alongside diesel. The lower premixed air excess ratio due to increasing MEF also deteriorates the mixing of diesel and air during ID. The resulting weaker and delayed Phase I results in the apparent lower peak pressure and PRR. At 11 bar gIMEP load point, P_{max} consistently decreases from 102.0 bar to 69.0 bar, with PRR_{max} dropping from 7.05 bar/°CA to 3.14 bar/°CA, even below the 4.54 bar/°CA in DO operation. The same decreasing trend is observed for both pressure metrics at the higher load, yet after the transition at 88% MEF, both start rising again. While peak pressures under methanol operation remain well below the peak pressure levels of DO due to the relatively delayed combustion phasing, peak PRRs are typically well above the DO baseline which is attributed to the observation of more concentrated combustion of fuel in less time for methanol DF.

Knock intensity emerges as a key parameter when transitioning from DO to methanol PRDF operation, primarily due to enhanced reactivity of the end-gas mixture during combustion. Knocking levels are higher across most MEFs investigated, with the most severe knock occurring at the lower end of the MEF range, a factor that ultimately

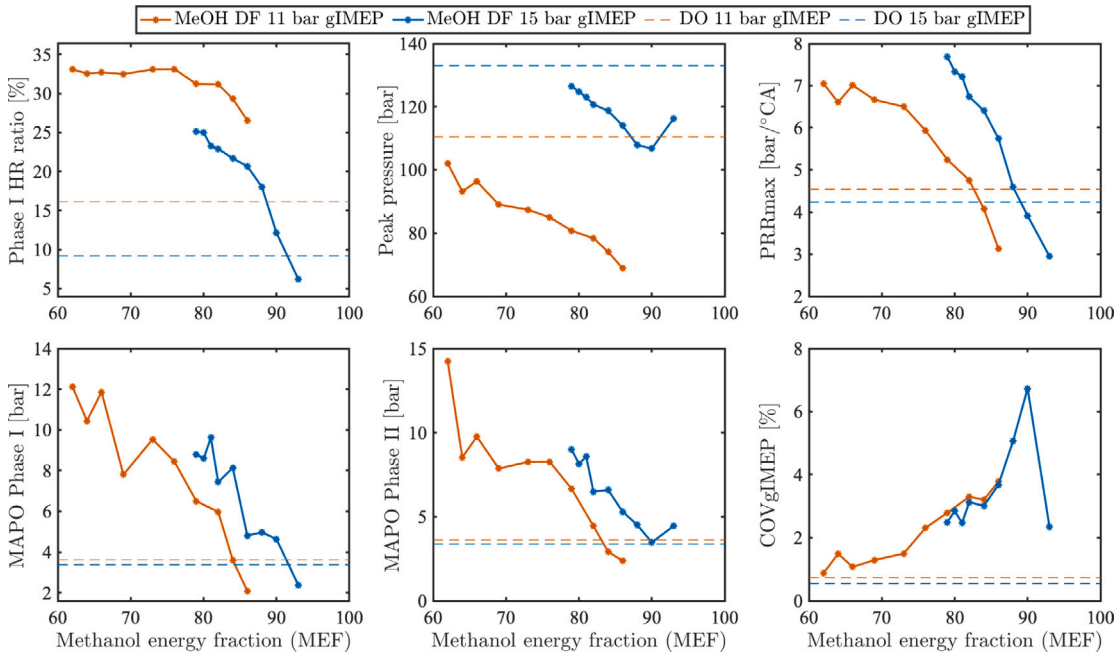

Fig. 19. Effect of MEF on combustion characteristics and stability for the two high-load points.

constrained the minimum MEF limit during the experimental campaign. As the MEF increases, the MAPO during both Phase I and II systematically declines, reflecting reduced knocking severity. This trend is attributed to the greater methanol-induced charge cooling, which lowers end-gas reactivity and knock propensity. At the highest MEFs studied, the MAPO for Phase I even drops below the DO baseline. Specifically, at 11 bar gIMEP, MAPO reduction is linked to delayed combustion phasing, despite enhanced HR_I, while at 15 bar gIMEP, the decrease is due to a less intense Phase I, despite combustion timing closely matching that of DO operation.

Apart from knocking, increased reliance on flame propagation as the dominant combustion mechanism at higher MEFs makes the in-cylinder processes inherently more sensitive to cycle-to-cycle variations, particularly under lean operating conditions. This sensitivity is evidenced by the rising trend of the COV_{gIMEP} as MEF increases. For instance, at 11 bar gIMEP, as the combustion mechanism shifts from premixed autoignition to slower flame propagation, MAPO declines but COV_{gIMEP} rises significantly—from 0.87% at 62% MEF to 3.78% at 86% MEF—surpassing the DO baseline of 0.74%. Such deterioration in combustion stability serves as a precursor to lower efficiencies and increased UHC emissions. It is important to note that a COV_{IMEP} threshold of 3% is typically regarded as a practical upper limit for acceptable stability in flame propagation regimes such as lean-burn SI engines [78,79]. For the lower load (11 bar gIMEP), this limit is surpassed after 79% MEF, indicating a transition to rough engine operation, while at higher load (15 bar gIMEP) it exceeds this threshold after 82% MEF. However, the transition to the MPDF-type of combustion under the maximum MEF (93%) and its combustion phasing improvements achieve an acceptable COV_{IMEP} of 2.35%; though it still remains considerably above the DO baseline value of 0.55%. The effect of combustion phasing and stability on performance across the MEF sweeps, including the behavior at the highest MEFs and the maximum load, is confirmed through the analysis of energy balance, as depicted in Fig. 20.

For both 11 bar and 15 bar gIMEP load points, the overall energy balance shifts similarly with increasing MEF, except for the distinct transition observed after 88% at the higher load due to increased intake temperature. Across the MEF sweep, gross indicated thermal efficiency (gITE) declines with increasing MEF, primarily due to deteriorating combustion phasing that occurs farther from TDC. This delayed and prolonged combustion is responsible for the observed increase in exhaust energy losses throughout the sweeps. Conversely, elevated MEFs enhance cooling, consistently reducing heat transfer losses to levels significantly lower than those seen in DO operation (approximately 20%). At 11 bar gIMEP, heat transfer losses decrease substantially—from 15.60% at 62% MEF to 9.79% at 86% MEF. A similar trend is evident at 15 bar gIMEP; however, beyond 88% MEF, heat transfer losses begin to rise again, peaking at 12.17% at 93% MEF due to higher air temperature which counteracts methanol's cooling effect. The combustion phasing switch after 88% MEF leads to recovery in performance: gITE and combustion efficiency reach their maxima of 45.32% and 92.70% at 93% MEF, respectively. These remain, however, below those of DO operation (47.54% and 98.79%). Notably, even at the optimal combustion phasing at 93% MEF, exhaust losses stay elevated compared to other MEFs and DO operation. This is attributed to the absence of most premixed autoignition in the overall combustion process at the highest MEFs, which shifts a larger fraction of fuel to burn during the later expansion phase, thereby reducing thermodynamic efficiency.

5.3.3. Emissions characteristics

Fig. 21 presents the engine-out emissions profiles for NO, NO_2, CO, and UHC across the two MEF sweeps investigated in this study. NO emissions were significantly reduced compared to DO operation at all tested MEF levels for both load sweeps. This reduction was less pronounced at the lower end of the MEF range at 11 bar gIMEP, owing to diminished charge-cooling from lower methanol quantities and more advanced combustion phasing near TDC. At 11 bar gIMEP, ISNO emissions steadily decreased from 5.88 g/kWh to 2.10 g/kWh as MEF increased, considerably lower than the DO baseline of 7.53 g/kWh. At 15 bar gIMEP, the benefit is even more substantial due to higher achieved MEFs, with ISNO emissions falling to as low as 1.07 g/kWh under methanol DF operation (compared to 7.53 g/kWh for DO). As anticipated, NO_2 emissions are higher at all MEF conditions relative to the DO baseline. Increasing MEF, however, resulted in lower levels of NO_2, which can be attributed to the lower levels of NO which reduces the NO density in the end-gas region during the end combustion phase.

The cooling effect of methanol and the increased reliance on flame propagation in PRDF mode generally produces a clear trade-off between

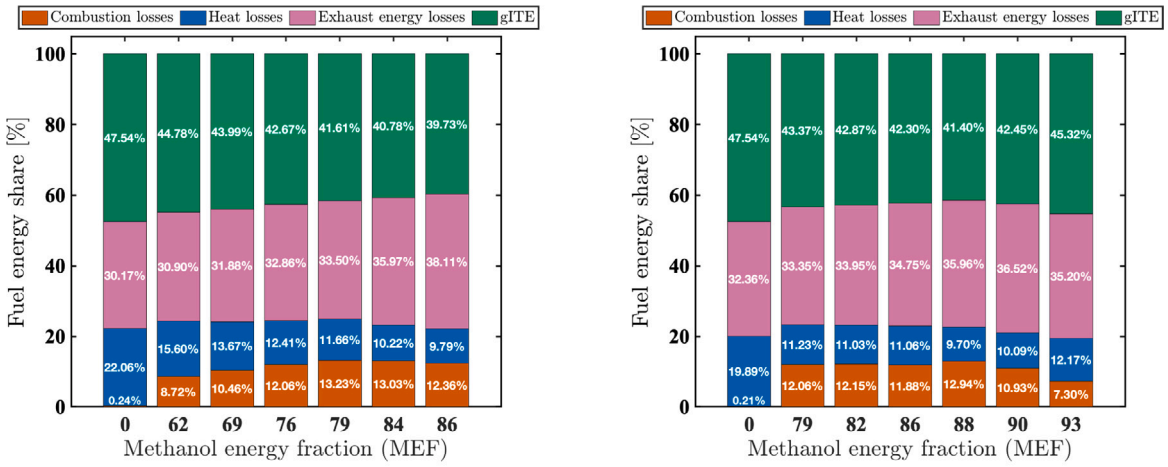

(a) 11 bar gIMEP **(b)** 15 bar gIMEP

Fig. 20. Effect of MEF on fuel's energy distribution for the two high-load points.

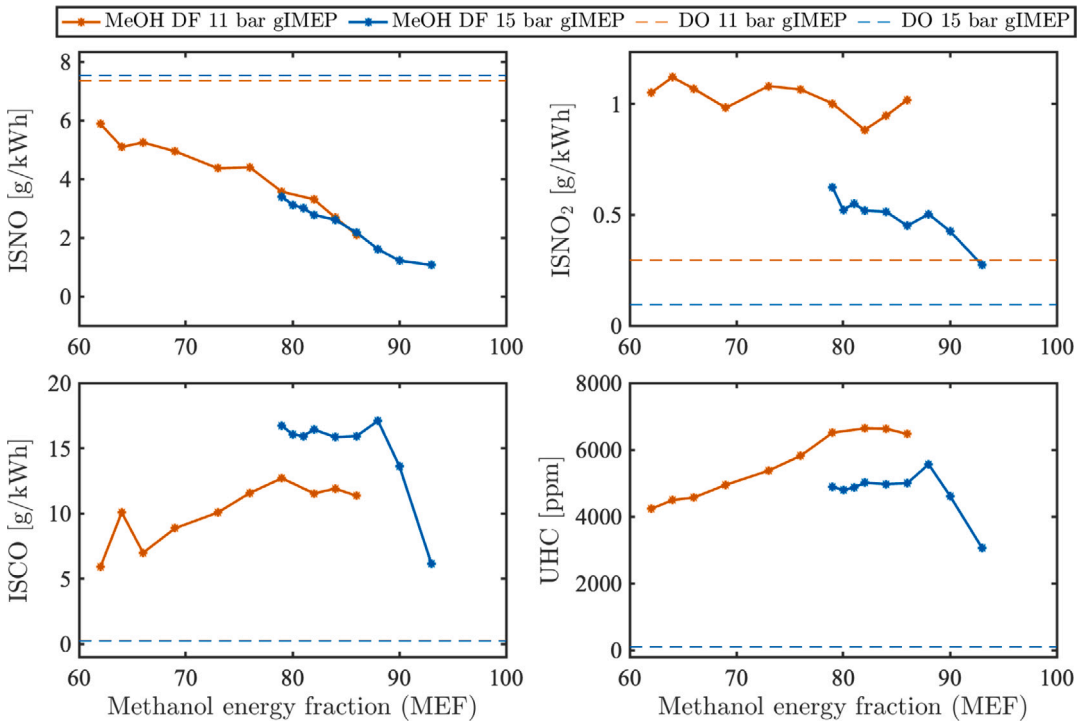

Fig. 21. Effect of MEF on emissions characteristics for the two high-load points.

NO_x and partial combustion products, i.e., higher CO and UHC emissions. For all MEFs assessed, CO and UHC levels far exceeded those of DO operation (with DO baselines at 0.23 g/kWh for CO and 97 ppm for UHC). At 11 bar gIMEP, ISCO rose from 5.88 g/kWh to 11.35 g/kWh, and UHC values increased from 4228 ppm to 6472 ppm with rising MEF. At 15 bar gIMEP, these emissions remained at relatively similar levels across the sweep, except a slight rise at 88% MEF. However, beyond 88% MEF, a remarkable drop occurs: ISCO falls from 17.1 g/kWh to 6.14 g/kWh at 93% MEF, with UHC also decreasing from 5567 ppm to 3061 ppm.

In summary, higher MEF in PRDF tends to lower NO emissions by reducing in-cylinder temperatures and diffusion combustion, but this benefit is offset by higher CO, UHC, and NO_2. Raising the intake air temperature at 93% MEF markedly improved emissions and overall performance, showing the strong influence of boundary conditions. Careful control of intake temperature can enhance PRDF performance, reduce pilot-fuel demand, and improve both emissions and efficiency. In practice, a viable concept will aim to balance MEF against emission targets and efficiency rather than seeking the highest MEF. The role of boundary conditions, such as air excess ratio and residual gas fractions, will be examined in a follow-up study.

6. Conclusions and recommendations

This study conducted an experimental investigation on a large-bore single-cylinder marine engine operating under the methanol premixed dual-fuel (PRDF) strategy at high methanol energy fractions (MEFs). By integrating qualitative and quantitative analytical frameworks, the research provides new insights into combustion mechanisms and phasing governing the process, and their relationships to overall engine performance. The main conclusions and recommendations are:

- Two distinct MEF operational windows were identified during the experimental campaign: the first limited at lower MEFs by excessive pressure rise and combustion instability, and the second bounded at higher MEFs by a renewed onset of instability and deteriorating combustion efficiency.
- The diesel-only (DO) to methanol dual-fuel (DF) transition fundamentally alters the energy balance. Heat transfer losses decreased by as much as 100% compared to DO, and although thermodynamic efficiency was slightly compromised, methanol operation enhanced the conversion of released fuel energy into work output. Nevertheless, the main barrier to maintain or even further improve the overall thermal efficiency of diesel engines with methanol remains the high combustion losses, as combustion efficiency dropped from 99.8% (DO) to 92.7% (PRDF) at the highest MEF and load tested.
- Qualitative analysis of heat release rate (HRR) profiles revealed three distinct combustion modes: (i) m-shape (Mode I)—a dual peak profile dominated by premixed autoignition for both fuels, (ii) h-shape (Mode II)—a pronounced pilot autoignition followed by attenuated flame propagation, and (iii) n-shape (Mode III)—dominated by turbulent bulk flame propagation at the highest MEFs and increasing air temperatures.
- A new methodology using the adopted metrics of Combustion Mechanism Index (CMI) and Phase Magnitude Ratio (PMR) was established to enable a systematic mapping and identification of combustion modes across the various HRR profiles. This framework also highlights the transitions in combustion behavior unique to methanol PRDF engines. Future advancements incorporating optical diagnostics and chemical kinetics modeling can further enhance the accuracy and applicability of this methodology, supporting improved engine control and performance.
- Combustion performance was found to be more sensitive to pilot ignition timing than to total ignition energy, mirroring conventional SI engine behavior. Even as the heat release from Phase I decreased (from 25% at 79% MEF to 6.2% at 93% MEF), advancing ignition by shortening ignition delay (from 9.2 °CA to 4.4 °CA) improved combustion efficiency (87.9% to 92.7%) and gross indicated thermal efficiency (43.4% to 45.3%).
- The observed boost in combustion efficiency at 93% MEF with increased intake temperature indicates a promising path to reduce combustion losses without raising heat transfer or NOx emissions. This is particularly important for existing diesel engines with mechanically driven injection systems, in which minimal modifications are sought in retrofitting scenarios. This highlights the scope for detailed parametric studies on such control parameters to further optimize methanol PRDF performance, which will be addressed in a future study.
- All methanol DF operating points resulted in lower NO_x emissions compared to DO (ISNO reduced from 7.53 g/kWh to as low as 1.07 g/kWh at peak MEF). This came at the cost of higher NO_2/NO ratios and substantial increases in CO and UHC emissions, yet these trade-offs diminished at the highest MEF, which achieved the best overall performance and emissions balance.

In summary, this work advances the understanding of high-MEF methanol PRDF combustion, clarifies its distinct operating modes, and introduces robust frameworks for combustion classification. The methodologies established here can be extended using broader operating ranges to enhance diagnostic and optimization strategies, supporting continued development of methanol-fueled heavy-duty powertrains and advancing the adoption of renewable fuels.

CRediT authorship contribution statement

Konstantinos I. Kiouranakis: Writing – original draft, Visualization, Methodology, Investigation, Formal analysis, Data curation, Conceptualization. **Robbert Willems:** Writing – review & editing, Methodology, Formal analysis, Data curation, Conceptualization. **Peter de Vos:** Writing – review & editing, Supervision, Conceptualization. **Rinze Geertsma:** Writing – review & editing, Project administration, Funding acquisition, Conceptualization.

Declaration of competing interest

The authors declare the following financial interests/personal relationships which may be considered as potential competing interests: Konstantinos Ioannis Kiouranakis reports financial support was provided by Netherlands Enterprise Agency. If there are other authors, they declare that they have no known competing financial interests or personal relationships that could have appeared to influence the work reported in this paper.

Acknowledgments

Present work is part of the MENENS project (Methanol als Energiestap Naar Emissieloze Nederlandse Scheepvaart). The project is funded by the Netherlands Enterprise Agency (RVO: Rijksdienst voor Ondernemend Nederland) under the grant number MOB21012. Gratitude is offered to the TNO engine lab team for providing us with the opportunity to work on this experimental research study together. The authors would like to thank dr.ir. Menno Merts for his time to review the manuscript and valuable comments that helped improve the quality of the manuscript. The Sankey diagrams are plotted using the scripts created by Liu [80]. The author acknowledges the use of Perplexity AI as a supervisory tool for grammar and readability. The tool was applied carefully, solely sentence by sentence where necessary, to enhance clarity and language without influencing the scientific content.

Data availability

The data that support the findings of this study are available from the corresponding author, upon reasonable request.

References

[1] Kalghatgi G, Agarwal AK, Leach F, Senecal K, editors. Engines and fuels for future transport. Energy, environment and sustainability, Singapore: Springer; 2022.
[2] Smil V. Numbers don't lie: 71 stories to help us understand the modern world. New York, New York: Penguin Books; 2021.
[3] Kalghatgi G. Is it really the end of internal combustion engines and petroleum in transport? Appl Energy 2018;225:965–74. http://dx.doi.org/10.1016/j.apenergy.2018.05.076.
[4] Curran S, Onorati A, Payri R, Agarwal AK, Arcoumanis C, Bae C, Boulouchos K, Dal Forno Chuahy F, Gavaises M, Hampson GJ, Hasse C, Kaul B, Kong S-C, Kumar D, Novella R, Pesyridis A, Reitz R, Vaglieco BM, Wermuth N. The future of ship engines: Renewable fuels and enabling technologies for decarbonization. Int J Engine Res 2023;14680874231187954. http://dx.doi.org/10.1177/14680874231187954, URL http://journals.sagepub.com/doi/10.1177/14680874231187954.
[5] Xing H, Stuart C, Spence S, Chen H. Alternative fuel options for low carbon maritime transportation: Pathways to 2050. J Clean Prod 2021;297:126651. http://dx.doi.org/10.1016/j.jclepro.2021.126651, URL https://linkinghub.elsevier.com/retrieve/pii/S0959652621008714.
[6] Verhelst S, Turner JW, Sileghem L, Vancoillie J. Methanol as a fuel for internal combustion engines. Prog Energy Combust Sci 2019;70:43–88. http://dx.doi.org/10.1016/j.pecs.2018.10.001, URL https://linkinghub.elsevier.com/retrieve/pii/S036012851830042X.
[7] Pu Y-H, Dejaegere Q, Svensson M, Verhelst S. Renewable methanol as a fuel for heavy-duty engines: A review of technologies enabling single-fuel solutions. Energies 2024;17(7):1719. http://dx.doi.org/10.3390/en17071719, URL https://www.mdpi.com/1996-1073/17/7/1719.
[8] Svanberg M, Ellis J, Lundgren J, Landälv I. Renewable methanol as a fuel for the shipping industry. Renew Sustain Energy Rev 2018;94:1217–28. http://dx.doi.org/10.1016/j.rser.2018.06.058.
[9] Tian Z, Wang Y, Zhen X, Liu Z. The effect of methanol production and application in internal combustion engines on emissions in the context of carbon neutrality: A review. Fuel 2022;320:123902. http://dx.doi.org/10.1016/j.fuel.2022.123902, URL https://linkinghub.elsevier.com/retrieve/pii/S001623612200761X.

[10] Zhen X, Wang Y. An overview of methanol as an internal combustion engine fuel. Renew Sustain Energy Rev 2015;52:477–93. http://dx.doi.org/10.1016/j.rser.2015.07.083, URL https://linkinghub.elsevier.com/retrieve/pii/S1364032115007303.

[11] Santasalo-Aarnio A, Nyari J, Wojcieszyk M, Kaario O, Kroyan Y, Magdeldin M, Larmi M, Järvinen M. Application of synthetic renewable methanol to power the future propulsion. 2020, http://dx.doi.org/10.4271/2020-01-2151, pp. 2020–01–2151. URL https://www.sae.org/content/2020-01-2151/.

[12] Latarche M, Pounder CC. Pounder's marine diesel engines and gas turbines. 10th ed. Oxford: Butterworth-Heinemann; 2021, OCLC: 1230930006.

[13] Persson H, Hultqvist A, Johansson B, Remón A. Investigation of the early flame development in spark assisted HCCI combustion using high speed chemiluminescence imaging. 2007, http://dx.doi.org/10.4271/2007-01-0212, pp. 2007–01–0212. URL https://www.sae.org/content/2007-01-0212/.

[14] Wissink M, Reitz RD. Direct dual fuel stratification, a path to combine the benefits of RCCI and PPC. SAE Int J Engines 2015;8(2):878–89. http://dx.doi.org/10.4271/2015-01-0856, URL https://www.sae.org/content/2015-01-0856/.

[15] Kiouranakis KI, De Vos P, Zoumpourlos K, Coraddu A, Geertsma R. Methanol for heavy-duty internal combustion engines: Review of experimental studies and combustion strategies. Renew Sustain Energy Rev 2025;214:115529. http://dx.doi.org/10.1016/j.rser.2025.115529, URL https://linkinghub.elsevier.com/retrieve/pii/S1364032125002023.

[16] International Chamber of Shipping. Fuelling the fourth propulsion revolution. Technical Report, 2022, URL https://www.ics-shipping.org/publication/fuelling-the-fourth-propulsion-revolution-an-opportunity-for-all-full-report/.

[17] Karim GA. Dual-fuel diesel engines. CRC Press; 2015, http://dx.doi.org/10.1201/b18163, URL https://www.taylorfrancis.com/books/9781498703093.

[18] Reitz RD, Duraisamy G. Review of high efficiency and clean reactivity controlled compression ignition (RCCI) combustion in internal combustion engines. Prog Energy Combust Sci 2015;46:12–71. http://dx.doi.org/10.1016/j.pecs.2014.05.003, URL https://linkinghub.elsevier.com/retrieve/pii/S0360128514000288.

[19] Kiouranakis KI, Vos PD, Geertsma R. Methanol as a fuel in shipping: Review and outlook to ICE research within MENENS. In: Transport transitions: advancing sustainable and inclusive mobility. Lecture Notes in Mobility, Springer Nature Switzerland; 2025, p. 735–42. http://dx.doi.org/10.1007/978-3-031-89444-2_106, URL https://link.springer.com/10.1007/978-3-031-89444-2_106.

[20] Yin X, Ren X, Wang J, Duan H, Hu E, Zeng K. Influence of methanol and diesel injection timings on the maximum methanol energy substitution ratio and performance of diesel/methanol dual-direct injection engine. Energy 2025;318:134762. http://dx.doi.org/10.1016/j.energy.2025.134762, URL https://linkinghub.elsevier.com/retrieve/pii/S0360544225004049.

[21] Wang Z, Du G, Wang D, Xu Y, Shao M. Combustion process decoupling of a diesel/natural gas dual-fuel engine at low loads. Fuel 2018;232:550–61. http://dx.doi.org/10.1016/j.fuel.2018.05.152, URL https://linkinghub.elsevier.com/retrieve/pii/S0016236118309797.

[22] Cung KD, Wallace J, Kalaskar V, Smith Iii EM, Briggs T, Bitsis Jr. DC. Experimental study on engine and emissions performance of renewable diesel methanol dual fuel (RMDF) combustion. Fuel 2024;357:129664. http://dx.doi.org/10.1016/j.fuel.2023.129664, URL https://linkinghub.elsevier.com/retrieve/pii/S0016236123022780.

[23] Dierickx J, Verbiest J, Janvier T, Peeters J, Sileghem L, Verhelst S. Retrofitting a high-speed marine engine to dual-fuel methanol-diesel operation: A comparison of multiple and single-point methanol port injection. Fuel Commun 2021;7:100010. http://dx.doi.org/10.1016/j.jfueco.2021.100010, URL https://linkinghub.elsevier.com/retrieve/pii/S2666052021000030.

[24] Zhao Y, Liu X, Kook S. Combustion mode evaluation of a methanol–diesel dual direct injection engine with a control of injection timing and energy substitution ratio. SAE Int J Engines 2024;18(1). http://dx.doi.org/10.4271/03-18-01-0002, 03–18–01–0002. URL https://www.sae.org/content/03-18-01-0002.

[25] Splitter D, Szybist J, Jatana G, Svensson K, Montgomery D. Approach for high methanol substitution by energy with conventional and bio pilot fuels. Zurich: CIMAC; 2025.

[26] Stenzel K, Thorau P, Beckmann L, Schirrmeister F, Reiser C, Buchholz B. Experimental investigations of a methanol dual-fuel combustion process for marine engines. Zurich: CIMAC; 2025.

[27] Wagemakers A, Leermakers C. Review on the effects of dual-fuel operation, using diesel and gaseous fuels, on emissions and performance. 2012, http://dx.doi.org/10.4271/2012-01-0869, pp. 2012–01–0869. URL https://www.sae.org/content/2012-01-0869/.

[28] Korakianitis T, Namasivayam A, Crookes R. Natural-gas fueled spark-ignition (SI) and compression-ignition (CI) engine performance and emissions. Prog Energy Combust Sci 2011;37(1):89–112. http://dx.doi.org/10.1016/j.pecs.2010.04.002, URL https://linkinghub.elsevier.com/retrieve/pii/S0360128510000377.

[29] McIlroy A, McRae G, Sick V, Siebers DL, Westbrook CK, Smith PJ, Taatjes C, Trouve A, Wagner AF, Rohlfing E, Manley D, Tully F, Hilderbrandt R, Green W, Marceau D, O'Neal J, Lyday M, Cebulski F, Garcia TR, Strong D. Basic research needs for clean and efficient combustion of 21st century transportation fuels. Technical Report, (935428):2006, 935428. http://dx.doi.org/10.2172/935428, URL http://www.osti.gov/servlets/purl/935428-bbBji1/.

[30] Maurya RK. Reciprocating engine combustion diagnostics: In-cylinder pressure measurement and analysis. 1st ed. 2019. Mechanical engineering series, Cham: Springer International Publishing : Imprint: Springer; 2019, http://dx.doi.org/10.1007/978-3-030-11954-6.

[31] Zhou L, Kang R, Wei H, Feng D, Hua J, Pan J, Chen R. Experimental analysis of super-knock occurrence based on a spark ignition engine with high compression ratio. Energy 2018;165:68–75. http://dx.doi.org/10.1016/j.energy.2018.09.166, URL https://linkinghub.elsevier.com/retrieve/pii/S0360544218319388.

[32] Gao J, Yao A, Feng L, Xu H, Yao C. Experimental investigation on the failures of engine piston subjected to severe knock. 2019, http://dx.doi.org/10.4271/2019-01-0705, pp. 2019–01–0705. URL https://www.sae.org/content/2019-01-0705/.

[33] Meininger RD, Kweon C-BM, Szedlmayer MT, Dang KQ, Jackson NB, Lindsey CA, Gibson JA, Armstrong RH. Knock criteria for aviation diesel engines. Int J Engine Res 2017;18(7):752–62. http://dx.doi.org/10.1177/1468087416669882, URL https://journals.sagepub.com/doi/10.1177/1468087416669882.

[34] Ahmad Z, Kaario O, Qiang C, Vuorinen V, Larmi M. A parametric investigation of diesel/methane dual-fuel combustion progression/stages in a heavy-duty optical engine. Appl Energy 2019;251:113191. http://dx.doi.org/10.1016/j.apenergy.2019.04.187, URL https://linkinghub.elsevier.com/retrieve/pii/S0306261919308505.

[35] Choi M, Mohiuddin K, Park S. Effects of methane ratio on MPDF (micro-pilot dual-fuel) combustion characteristic in a heavy-duty single cylinder engine. Sci Rep 2021;11(1):9740. http://dx.doi.org/10.1038/s41598-021-89161-z, URL https://www.nature.com/articles/s41598-021-89161-z.

[36] Li W, Liu Z, Wang Z. Experimental and theoretical analysis of the combustion process at low loads of a diesel natural gas dual-fuel engine. Energy 2016;94:728–41. http://dx.doi.org/10.1016/j.energy.2015.11.052, URL https://linkinghub.elsevier.com/retrieve/pii/S0360544215016114.

[37] Benajes J, García A, Monsalve-Serrano J, Boronat V. Gaseous emissions and particle size distribution of dual-mode dual-fuel diesel-gasoline concept from low to full load. Appl Therm Eng 2017;120:138–49. http://dx.doi.org/10.1016/j.applthermaleng.2017.04.005, URL https://linkinghub.elsevier.com/retrieve/pii/S1359431117308037.

[38] Lounici M, Benbellil M, Loubar K, Niculescu D, Tazerout M. Knock characterization and development of a new knock indicator for dual-fuel engines. Energy 2017;141:2351–61. http://dx.doi.org/10.1016/j.energy.2017.11.138, URL https://linkinghub.elsevier.com/retrieve/pii/S0360544217319965.

[39] Azimov U, Tomita E, Kawahara N, Harada Y. Premixed mixture ignition in the end-gas region (PREMIER) combustion in a natural gas dual-fuel engine: operating range and exhaust emissions. Int J Engine Res 2011;12(5):484–97. http://dx.doi.org/10.1177/1468087411409664, URL https://journals.sagepub.com/doi/10.1177/1468087411409664.

[40] Xu C, Zhuang Y, Qian Y, Cho H. Effect on the performance and emissions of methanol/diesel dual-fuel engine with different methanol injection positions. Fuel 2022;307:121868. http://dx.doi.org/10.1016/j.fuel.2021.121868.

[41] Imamoto T, Kawahara N, Tomita E. PREMIER combustion characteristics of a pilot fuel-ignited dual-fuel biogas engine with consideration of cycle-to-cycle variations. Fuel 2022;314:123049. http://dx.doi.org/10.1016/j.fuel.2021.123049, URL https://linkinghub.elsevier.com/retrieve/pii/S0016236121029094.

[42] Azimov U, Tomita E, Kawahara N, Harada Y. Effect of syngas composition on combustion and exhaust emission characteristics in a pilot-ignited dual-fuel engine operated in PREMIER combustion mode. Int J Hydrog Energy 2011;36(18):11985–96. http://dx.doi.org/10.1016/j.ijhydene.2011.04.192, URL https://linkinghub.elsevier.com/retrieve/pii/S0360319911010895.

[43] Papagiannakis R, Hountalas D. Experimental investigation concerning the effect of natural gas percentage on performance and emissions of a DI dual fuel diesel engine. Appl Therm Eng 2003;23(3):353–65. http://dx.doi.org/10.1016/S1359-4311(02)00187-4, URL https://linkinghub.elsevier.com/retrieve/pii/S1359431102001874.

[44] Dierickx J, Mattheeuws L, Christianen K, Stenzel K, Verhelst S. Evaluation and extension of ignition delay correlations for dual-fuel operation with hydrogen or methanol in a medium speed single cylinder engine. Fuel 2023;345:128254. http://dx.doi.org/10.1016/j.fuel.2023.128254, URL https://linkinghub.elsevier.com/retrieve/pii/S0016236123008670.

[45] Xu H, Yao C, Xu G. Chemical kinetic mechanism and a skeletal model for oxidation of n-heptane/methanol fuel blends. Fuel 2012;93:625–31. http://dx.doi.org/10.1016/j.fuel.2011.09.048, URL https://linkinghub.elsevier.com/retrieve/pii/S0016236111006089.

[46] Pan W, Yao C, Han G, Wei H, Wang Q. The impact of intake air temperature on performance and exhaust emissions of a diesel methanol dual fuel engine. Fuel 2015;162:101–10. http://dx.doi.org/10.1016/j.fuel.2015.08.073.

[47] Kim K, Szedlmayer M, Kruger K, Kweon C. Optimization of in-cylinder pressure filter for engine research. Technical Report, US Army Research Laboratory; 2017.

[48] The MathWorks Inc. MATLAB version: 24.2.0 (R2024b). 2023, URL https://www.mathworks.com.

[49] Wallner T. Correlation between speciated hydrocarbon emissions and flame ionization detector response for gasoline/alcohol blends. J Eng Gas Turbines Power 2011;133(8):082801. http://dx.doi.org/10.1115/1.4002893, URL https://asmedigitalcollection.asme.org/gasturbinespower/article/doi/10.1115/1.4002893/408142/Correlation-Between-Speciated-Hydrocarbon.

[50] Thermo Electron Scientific. The measurement of methanol and formaldehyde in automobile exhaust using Fourier transform infrared (FT-IR) spectroscopy. Technical Report, Thermo Electron Scientific Instruments LLC, URL https://assets.thermofisher.com/TFS-Assets/CAD/Application-Notes/AN50652-E-Measurement-Methanol-Formaldehyde-Auto-Exhaust.pdf.

[51] Wei H, Zhang Z, Zhang X, Dong F, Yuan W, Chen H. Overview for methanol and formaldehyde unregulated emissions of methanol fueled engines. J Energy Inst 2025;120:102089. http://dx.doi.org/10.1016/j.joei.2025.102089, URL https://linkinghub.elsevier.com/retrieve/pii/S1743967125001175.

[52] Stapersma D. Diesel engines: A fundamental approach to performance analysis, turbocharging, combustion, emissions and heat transfer : Including thermodynamical principles. Vol. 3: Combustion. vol. 1, TU Delft; 2009, URL https://books.google.gr/books?id=Bpq7nQEACAAJ.

[53] Heywood JB. Internal combustion engine fundamentals. 2nd ed. New York: McGraw-Hill Education; 2018.

[54] Burcat A, Ruscic B, Chemistry. Third millenium ideal gas and condensed phase thermochemical database for combustion (with update from active thermochemical tables). Technical Report, (ANL-05/20, 925269):2005, 925269.

[55] Yun HJ, Mirsky W. Schlieren-streak measurements of instantaneous exhaust gas velocities from a spark-ignition engine. 1974, 741015. http://dx.doi.org/10.4271/741015, URL https://www.sae.org/content/741015/.

[56] Maldonado BP, Kaul BC. Evaluation of residual gas fraction estimation methods for cycle-to-cycle combustion variability analysis and modeling. Int J Engine Res 2022;23(2):198–213. http://dx.doi.org/10.1177/1468087420983087, URL https://journals.sagepub.com/doi/10.1177/1468087420983087.

[57] Woschni G. A universally applicable equation for the instantaneous heat transfer coefficient in the internal combustion engine. In: SAE technical paper 670931, 1967, http://dx.doi.org/10.4271/670931.

[58] Guezennec YG, Hamama W. Two-zone heat release analysis of combustion data and calibration of heat transfer correlation in an I. C. engine. In: SAE technical paper 1999-01-0218, 1999, http://dx.doi.org/10.4271/1999-01-0218.

[59] Li Y, Zhang C, Yu W, Wu H. Effects of rapid burning characteristics on the vibration of a common-rail diesel engine fueled with diesel–methanol dual-fuel. Fuel 2016;170:176–84. http://dx.doi.org/10.1016/j.fuel.2015.12.045, URL https://linkinghub.elsevier.com/retrieve/pii/S001623611501306X.

[60] Ma B, Yao A, Yao C, Chen C, Qu G, Wang W, et al. Multiple combustion modes existing in the engine operating in diesel methanol dual fuel. Energy 2021;234:121285. http://dx.doi.org/10.1016/j.energy.2021.121285.

[61] Vressner A, Lundin A, Christensen M, Tunest° al P, Johansson B. Pressure oscillations during rapid HCCI combustion. 2003, http://dx.doi.org/10.4271/2003-01-3217, pp. 2003–01–3217. URL https://www.sae.org/content/2003-01-3217/.

[62] Suijs W, De Graeve R, Verhelst S. An exploratory study of knock intensity in a large-bore heavy-duty methanol engine. Energy Convers Manage 2024;302:118089. http://dx.doi.org/10.1016/j.enconman.2024.118089, URL https://linkinghub.elsevier.com/retrieve/pii/S019689042400030X.

[63] Lowe DP, Lin TR, Wu W, Tan ACC. Diesel knock combustion and its detection using acoustic emission. URL https://www.ndt.net/article/jae/papers/29-078.pdf.

[64] Woud HK, Stapersma D. Design of propulsion and electric power generation systems. iMarEST publications, London: Imarest; 2002.

[65] Wang B, Yao A, Yao C, Chen C, Wang H. In-depth comparison between pure diesel and diesel methanol dual fuel combustion mode. Appl Energy 2020;278:115664. http://dx.doi.org/10.1016/j.apenergy.2020.115664, URL https://linkinghub.elsevier.com/retrieve/pii/S0306261920311600.

[66] Huang Q, Yang R, Liu J, Xie T, Liu J. Investigation of the mechanism behind the surge in nitrogen dioxide emissions in engines transitioning from pure diesel operation to methanol/diesel dual-fuel operation. Fuel Process Technol 2024;264:108131. http://dx.doi.org/10.1016/j.fuproc.2024.108131, URL https://linkinghub.elsevier.com/retrieve/pii/S0378382024001012.

[67] Li Y, Li H, Guo H, Li Y, Yao M. A numerical investigation on NO2 formation in a natural gas–diesel dual fuel engine. J Eng Gas Turbines Power 2018;140(9):092804. http://dx.doi.org/10.1115/1.4039734, URL https://asmedigitalcollection.asme.org/gasturbinespower/article/doi/10.1115/1.4039734/367389/A-Numerical-Investigation-on-NO2-Formation-in-a.

[68] Lu H, Yao A, Yao C, Chen C, Wang B. An investigation on the characteristics of and influence factors for NO2 formation in diesel/methanol dual fuel engine. Fuel 2019;235:617–26. http://dx.doi.org/10.1016/j.fuel.2018.08.061, URL https://linkinghub.elsevier.com/retrieve/pii/S0016236118314327.

[69] Lee J, Chu S, Min K, Kim M, Jung H, Kim H, Chi Y. Classification of diesel and gasoline dual-fuel combustion modes by the analysis of heat release rate shapes in a compression ignition engine. Fuel 2017;209:587–97. http://dx.doi.org/10.1016/j.fuel.2017.07.067, URL https://linkinghub.elsevier.com/retrieve/pii/S0016236117309298.

[70] Wei L, Yao C, Wang Q, Pan W, Han G. Combustion and emission characteristics of a turbocharged diesel engine using high premixed ratio of methanol and diesel fuel. Fuel 2015;140:156–63. http://dx.doi.org/10.1016/j.fuel.2014.09.070, URL https://linkinghub.elsevier.com/retrieve/pii/S0016236114009399.

[71] Wannatong K, Akarapanyavit N, Siengsanorh S, Chanchaona S. Combustion and knock characteristics of natural gas diesel dual fuel engine. 2007, http://dx.doi.org/10.4271/2007-01-2047, pp. 2007–01–2047. URL https://www.sae.org/content/2007-01-2047/.

[72] Zhou L, Hua J, Wei H, Dong K, Feng D, Shu G. Knock characteristics and combustion regime diagrams of multiple combustion modes based on experimental investigations. Appl Energy 2018;229:31–41. http://dx.doi.org/10.1016/j.apenergy.2018.07.102, URL https://linkinghub.elsevier.com/retrieve/pii/S0306261918311383.

[73] Willems R, Willems F, Deen N, Somers B. Heat release rate shaping for optimal gross indicated efficiency in a heavy-duty RCCI engine fueled with e85 and diesel. Fuel 2021;288:119656. http://dx.doi.org/10.1016/j.fuel.2020.119656, URL https://linkinghub.elsevier.com/retrieve/pii/S0016236120326521.

[74] Wang Z, Su X, Wang X, Jia D, Wang D, Li J. Impact of ignition energy on the combustion performance of an SI heavy-duty stoichiometric operation natural gas engine. Fuel 2022;313:122857. http://dx.doi.org/10.1016/j.fuel.2021.122857, URL https://linkinghub.elsevier.com/retrieve/pii/S0016236121027198. Publisher: Elsevier BV.

[75] Zhang X, Chen L. The synergy effect of ignition energy and spark plug gap on methane lean combustion with addressing initial flame formation and cyclic variation. ACS Omega 2023;8(7):7036–44. http://dx.doi.org/10.1021/acsomega.2c07897, URL https://pubs.acs.org/doi/10.1021/acsomega.2c07897. Publisher: American Chemical Society (ACS).

[76] Olsson K, Johansson B. Combustion chambers for natural gas SI engines part 2: Combustion and emissions. 1995, 950517. http://dx.doi.org/10.4271/950517, URL https://www.sae.org/content/950517/.

[77] Kiouranakis K, De Vos P, Willems R, Sapra H, Geertsma R. Heat release behavior in a converted marine natural gas SI engine: Exploring the impact of bowl-in and squish phases on performance and emissions. J Appl Therm Eng 2025. Manuscript submitted for publication.

[78] Jones MGK, Heaton DM. Nebula combustion system for lean burn spark ignited gas engines. In: SAE technical paper 890211, 1989, http://dx.doi.org/10.4271/890211.

[79] Kiouranakis KI, De Vos P, Sapra H, Geertsma R. Natural gas for marine lean-burn spark ignition engines: A combustion stability analysis. In: ASME 2024 ICE forward conference. San Antonio, Texas, USA: American Society of Mechanical Engineers; 2024, http://dx.doi.org/10.1115/icef2024-139218, URL https://asmedigitalcollection.asme.org/ICEF/proceedings/ICEF2024/88520/V001T01A002/1210128.

[80] Liu Z. Sankey plot. 2025, URL https://www.mathworks.com/matlabcentral/fileexchange/128679-sankey-plot. MATLAB Central File Exchange, Copyright (c) 2023.